Electron

WILEY

Electron
Open Access

REVIEW OPEN ACCESS

Nanowire-Based Flexible Sensors for Wearable Electronics, Brain–Computer Interfaces, and Artificial Skins

Xiaopan Song[1] | Yang Gu[2] | Sheng Wang[2] | Junzhuan Wang[1] | Linwei Yu[1]

[1]School of Electronics Science and Engineering, Nanjing University, Nanjing, China | [2]School of Future Science and Engineering, Soochow University, Suzhou, China

Correspondence: Linwei Yu (yulinwei@nju.edu.cn) | Sheng Wang (shengwang@suda.edu.cn)

Received: 30 October 2024 | **Revised:** 14 December 2024 | **Accepted:** 3 January 2025

Funding: Financial support received from the National Key Research Program of China (No. 92164201), National Natural Science Foundation of China for Distinguished Young Scholars (No. 62325403), Natural Science Foundation of Jiangsu Province (BK20230498), Jiangsu Funding Program for Excellent Postdoctoral Talent (2024ZB427), and the National Natural Science Foundation of China (61934004).

Keywords: artificial skins | brain–computer interfaces | flexible sensors | nanowire | wearable electronics

ABSTRACT

Flexible electronic devices with compliant mechanical deformability and electrical reliability have been a focal point of research over the past decade, particularly in the fields of wearable devices, brain–computer interfaces (BCIs), and electronic skins. These emerging applications impose stringent requirements on flexible sensors, necessitating not only their ability to withstand dynamic strains and conform to irregular surfaces but also to ensure long-term stable monitoring. To meet these demands, one-dimensional nanowires, with high aspect ratios, large surface-to-volume ratios, and programmable geometric engineering, are widely regarded as ideal candidates for constructing high-performance flexible sensors. Various innovative assembly techniques have enabled the effective integration of these nanowires with flexible substrates. More excitingly, semiconductor nanowires, prepared through low-cost and efficient catalytic growth methods, have been successfully employed in the fabrication of highly flexible and stretchable nanoprobes for intracellular sensing. Additionally, nanowire arrays can be deployed on the cerebral cortex to record and analyze neural activity, opening new avenues for the treatment of neurological disorders. This review systematically examines recent advancements in nanowire-based flexible sensing technologies applied to wearable electronics, BCIs, and electronic skins, highlighting key design principles, operational mechanisms, and technological milestones achieved through growth, assembly, and transfer processes. These developments collectively advance high-performance health monitoring, deepen our understanding of neural activities, and facilitate the creation of novel, flexible, and stretchable electronic skins. Finally, we also present a summary and perspectives on the current challenges and future opportunities for nanowire-based flexible sensors.

1 | Introduction

Sensing technologies have been extensively researched for applications in the fields of mobile phones, autonomous driving cars, and health monitoring watches because of their diverse and significant benefits. Traditional sensors are typically fabricated from brittle and rigid materials, such as metals and semiconductors, which often exhibit poor mechanical properties [1–4]. Notably, in scenarios requiring bending, conforming to irregular surfaces, or enduring rapid and intense movements, these rigid materials are susceptible to internal fractures [5]. Such fractures can compromise the performance and stability of

Xiaopan Song and Yang Gu contributed equally to this study.

the sensors, making them unsuitable for the evolving demands of flexible sensing technologies. Besides, these sensors often need to be worn directly on the body to meet the requirements for long-term monitoring of various physiological parameters without causing discomfort, requiring high biocompatibility [6–8] and low Young's modulus [9–11]. To address these limitations, advancements in sensor technology over the past decade have primarily focused on novel structural designs and material innovations. By thinning bulk rigid materials and reducing them to nanostructures, the mechanical flexibility of these materials is significantly enhanced, better adapting them to the field of flexible sensing and monitoring, as well as to the requirements of flexible and stretchable electronic devices [12–14].

For example, typical two-dimensional (2D) thin-film structures have been extensively studied and utilized as active channels or conductive electrodes in flexible sensing applications [15–17]. Conductive organic thin films can be employed to fabricate various stretchable electronic devices, optoelectronic sensors, and display prototypes [18–21]. However, their relatively low conductivity and instability, which tend to degrade under prolonged exposure to air/moisture environments or continuous ultraviolet (UV) illumination, remain major concerns for practical and scalable applications [22–26]. In contrast, inorganic thin-film materials are more robust, offering higher stability. Thin-metal films, because of their simple fabrication process and abundant raw materials, are widely used as the sensitive layer and electrodes in flexible sensors. However, they are not suitable for environments that require mechanical strain, such as stretching, and even when reduced to nanoscale thickness they remain opaque. Indium-tin-oxide (ITO) thin films, with their high transparency and conductivity, are considered ideal for the fabrication of flexible display devices [27–29]. However, ITO is inherently brittle and rigid, making it difficult to adapt to more complex stretchable substrate surfaces [30, 31]. To enhance the flexibility of rigid inorganic materials, geometric design is a wise approach. Specifically, one-dimensional (1D) nanostructures, such as nanowires, can be grown and assembled into elastic configurations. This approach significantly reduces stress concentration, enhances the material's stretchability and mechanical flexibility, and allows for better adaptation to irregular surfaces in sensing applications. Meanwhile, we have summarized a simple comparison of the properties of 2D and 1D materials in Table 1.

In recent years, the integration of nanowire structures with flexible substrates as a crucial component of flexible sensors has made a significant progress. For instance, metal nanowires, including silver nanowires (AgNWs) and copper nanowires (CuNWs), have been widely adopted because of their excellent conductivity and the simplicity and efficiency of their synthesis methods, such as electrochemical [41], wet chemical [42], and polyol methods [43]. AgNWs exhibit superior durability [38, 44, 45] and excellent biocompatibility, making them an ideal choice for high-performance electrodes in long-term physiological signal monitoring, with broad applications in brain–computer interfaces (BCIs) and medical diagnostics. Furthermore, nanowire networks exhibit excellent mechanical stability and recoverability. Unlike thin films, these networks can deform and then reconstruct to regain their mechanical and electrical properties after being subjected to stress [46]. This characteristic is particularly beneficial for applications requiring repeated stretching or bending. On the other hand, CuNWs, with their good catalytic ability and cost-effectiveness, are suitable for biosensing applications [47, 48]. The high aspect ratio of nanowires allows them to withstand large mechanical strains without performance degradation, and by adjusting the density of nanowires tunable optical transparency can be achieved [39, 49–51]. In parallel, semiconductor nanowires, with their unique physicochemical properties [40, 52, 53], show great potential in enhancing the performance of flexible sensors [54, 55]. Silicon, as the most mature and reliable semiconductor material, serves as the backbone of microelectronic technology, providing a robust and cost-effective platform. Crystalline silicon nanowire (c-SiNWs) structures, used as sensing layers, have been extensively researched [56–58]. Currently, nanowires can be mass-produced using top–down etching methods [59]. However, these methods often require expensive electron beam lithography (EBL) and extreme ultraviolet (EUV) lithography equipment [60–62], significantly increasing costs. Therefore, it is of great significance to explore new strategies that can overcome the limitations of lithography for the fabrication of SiNW structures.

Bottom–up growth methods represent another effective approach for fabricating nanowire structures. Among these, the

TABLE 1 | Comparison between 2D and 1D materials.

Materials	Mechanical properties	Optical properties	Electrical properties	Stability	References
Organic film	Excellent stretchability and bendability	Optically transparent	Low electron mobility	Vulnerable to the external surrounding	[25, 32]
Transition metal carbides and nitrides	Excellent stretchability and bendability	Optically transparent	High electrical conductivity	Vulnerable to the external surrounding	[33–35]
Indium-tin-oxide	Unsuitable for stretchability and bendability	Optically transparent	High electrical conductivity	Stable	[27, 36]
Metal film	Unsuitable for stretchability	Relatively poor optical transparency	High electrical conductivity	Properties determined by the material	[15, 37]
Nanowires	Excellent stretchability and bendability	Tunable optically transparent	Unique electrical conductivity	Stable	[38–40]

conventional vapor–liquid–solid (VLS) method is one of the most widely used techniques, having been applied to produce various high-performance sensor prototypes [63–66]. This method utilizes catalytic droplets to absorb gaseous precursors, leading to the growth of nanowires at certain temperatures. Nevertheless, this low-cost and efficient manufacturing method faces significant challenges in precisely controlling the diameter and placement of nanowires and in freely designing their morphology. Recently, a novel in-plane solid–liquid–solid (IPSLS) mechanism has been extensively studied. Unlike VLS, using amorphous silicon (a-Si) as the precursor and low-melting-point metals (such as indium, tin, or gallium) as catalytic particles, the metal droplets can be continuously driven to move and absorb the front end of the solid a-Si layer at a relatively low temperature without any gaseous supply, thereby precipitating c-SiNWs at the rear end [67–71]. In this process, the introduction of a simple step edge can guide the growth of nanowires [72–75]. The strong interaction between the catalytic droplet and the absorption and deposition interfaces during the growth process enables effective control over the morphology of SiNWs [76]. Large-area spring-shaped [77, 78], mesh-shaped [79], specific letter-shaped [80, 81], and bio-probe-shaped [82] SiNWs have already been fabricated, laying a significant theoretical and experimental foundation for the positioning integration and flexible sensing applications of c-SiNWs.

Herein, we believe that nanowire-based flexible sensors possess excellent potential and a wide range of applications. Our review will be timely and of great interest to a broad readership. Specifically, we will focus on the latest progress in the fabrication of nanowires and novel nanowire-based flexible sensors mainly applied in the field of wearable electronics, BCI, and artificial skin. These advancements are of great chance to change the lifestyle of the human. This review is divided into the following sections. Following the introduction given in Section 1, we will start by introducing typical materials of nanowires and an overview of top–down and bottom–up synthesis methods and mechanisms and different methods for transferring nanowires to flexible substrates in Section 2. Then, in Section 3–5, we will introduce some typical or emerging nanowire-based flexible sensors' applications with different functions, such as pressure sensing, physiological parameters monitoring, tactile sensing, neuro probe, electroencephalogram (EEG) monitoring, and so on, widely applied in the field of wearable electronics, BCI, and artificial skin as illustrated in Figure 1, along with their structures and principles, in sequence. Finally, we will review the challenges faced by current systems and explore the future opportunities of nanowire-based flexible sensors and conclude this paper in Section 4.

2 | Fabrication Techniques of Nanowires

2.1 | Top–Down Methods

In top–down methods, optical lithography is an important and widely applied technique because of the rapid development of the semiconductor industry, which provides advanced equipment and established standards. Improving the resolution of lithography has consistently been a matter of significant

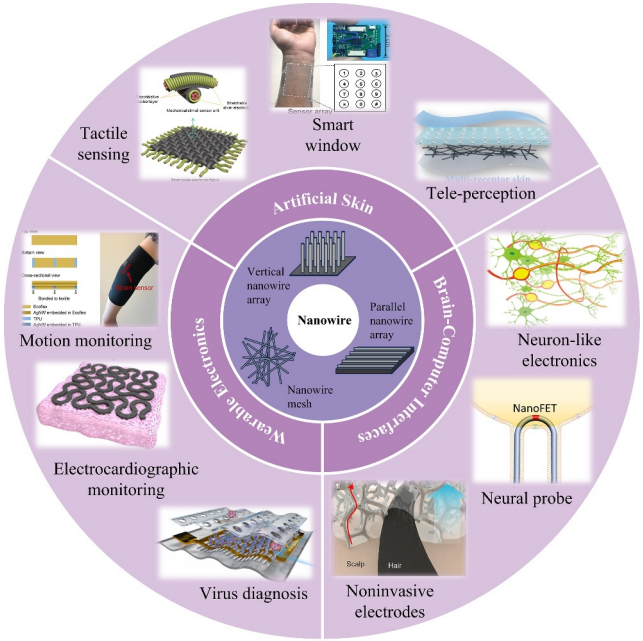

FIGURE 1 | Typical examples of nanowire-based flexible sensors application in the field of wearable electronics, BCIs, and artificial skins.

attention. The core of the issue can be derived from the following equation: the Rayleigh criterion [83].

$$D = \frac{k\lambda}{A}. \tag{1}$$

Critical dimension (D) represents the minimum critical dimension which can be distinguished under the influence of diffraction. Parameter k represents a process latitude factor and λ is the wavelength of the emission light. Besides, the numerical aperture (A) represents the numerical aperture and equals to $n\sin\theta$, where n represents the refractive index of the medium and θ represents the half angle of the maximum cone of light. From the above equation, it's obvious that the smaller the D, the higher the resolution of lithography. Therefore, reducing k and λ and enhancing A is of great importance to improve the precision. k is a parameter influenced by the manufacturing process. High-resolution resists and resist trimming processes can be used to reduce k values efficiently [84, 85]. However, it's still not sufficient for the current very large-scale integration circuit with high feature densities. Therefore, further process developments have been proposed to further reduce k, such as optical proximity correction [86], phase shift masks [87], off-axis illumination [88], multiple exposure [89], and so on. Although there have been many discussions about reducing k, it's hard to reduce k to a particularly small degree since k is already quite small. Therefore, improving A is also an important method to enhance the resolution. Improving the projection lens system can help increase the incident angle θ, and the roadmap of the innovation of the lens system is from spherical mirrors to aspherical mirrors to catadioptric systems. Since the incident angle θ has been raised to the theoretical limit, the refractive index of the medium n is also emphasized. Compared to conventional lithography, immersion lithography replaces the medium from air to liquid whose refractive index can exceed 1,

which can further decrease D [90]. Finally, the wavelength of the emission light λ is the most important and most concerning factor. The wavelength of the light source used in photolithography machines has evolved from early UV sources, such as g-line (wavelength 436 nm) and i-line (wavelength 365 nm), to DUV sources represented by KrF (wavelength 248 nm) and ArF (wavelength 193 nm), and now to EUV sources with a wavelength of 13.5 nm. The reduction of wavelength brings high resolution, but also more critical challenges. EUV is strongly absorbed by the medium, so it is only suitable for operating in vacuum. Therefore, novel lithography techniques have been proposed, such as EBL, x-ray lithography (XRL), and nanoimprint lithography (NIL).

Since the development of optical lithography techniques, they have been widely used in fabricating conductor nanowires. Pan et al. [91] employed a standard lithography to form an array of photoresist dots with designed diameter, and then evaporated a gold film as a catalyst in order to assist in etching a nanowire array (Figure 2B). In this work, using lithography they successfully produced large-scale ordered arrays of SiNWs, which were under precise control over diameters, lengths, spacings, and locations. However, the low resolution of standard lithography limits the diameters of nanowires which are over 400 nm. Therefore, lithography methods with higher resolution have been considered, such as EBL and XRL. Hashemi et al. [92] used EBL to fabricate SiNWs with diameters down to 8 nm as the channel of the gate-all-around (GAA) (Figure 2C), and Vladimirsky et al. [97] have utilized XRL to fabricate SiNWs with diameters down to 25 nm successfully. Besides, NIL is also a novel high-resolution method to fabricate nanowires. Küpers et al. [93] combine NIL with an indirect pattern transfer to fabricate holes on the substrate with a size down to 50 nm, which is provided for nanowire growth (Figure 2D). Among the above fabrication methods, EBL takes a leading role because the stamps of NIL and the mask patterns of DUV, EUV, and XRL are always fabricated by EBL techniques which theoretically limits the resolution of the latter two methods. However, EBL and XRL still face many problems, which hinder large-scale application and mass production, such as low wafer throughput and the trade-off between the stability and resolution of resist. Compared to the sequential process of EBL, NIL can be faster for large pattern sizes because of its parallel processing.

Different from the aforementioned lithography techniques, the template method is also a significant technical branch of top–down fabrication methods. For metallic nanowires, templates are employed to absorb the amount of metallic ions and restrict the growth of nanowires in order to control the morphology. There are various templates which can be mainly divided into hard templates such as porous alumina, mesoporous silica, and carbon nanotubes, and soft templates, such as DNA, proteins, and so on [94]. Figure 2D shows a schematic diagram of the synthesis of AgNWs by microtubule templates. Instead of synthesizing a single nanowire, template methods can also be applied to prepare a whole nanowire network and a nanowire array. Guo et al. [95] innovatively used grain-boundary lithography to form In islands as a template to control the growth of metallic nanowire networks (Figure 2F). In this work, compared to traditional methods using the process of welding metallic nanowires into nanowire networks [98], the contact between

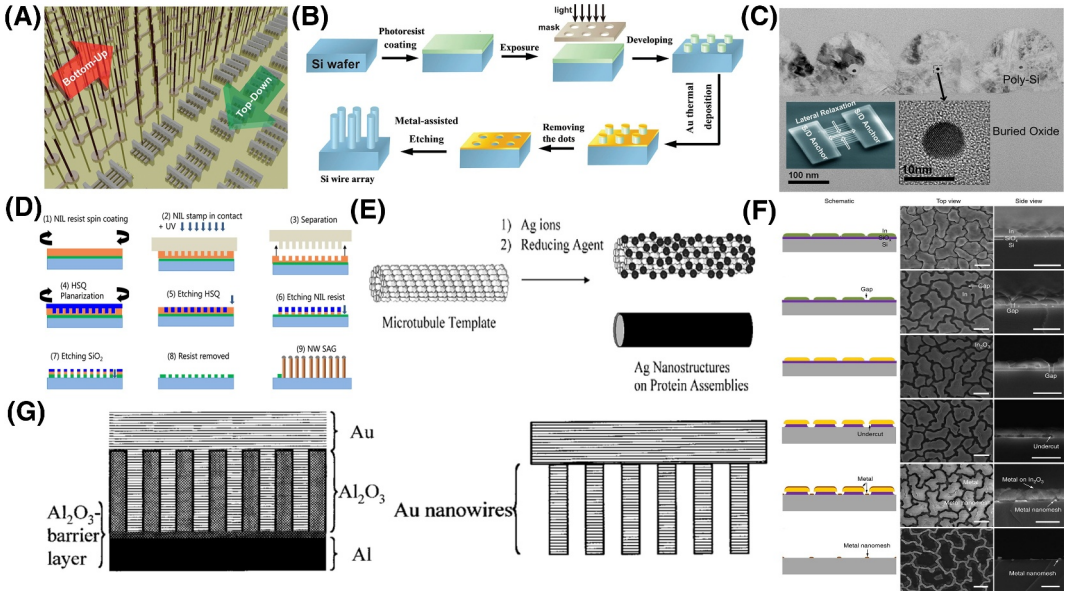

FIGURE 2 | (A) These nanowire fabrication routes can usually be categorized into two paradigms: bottom–up or top–down [59]. Reproduced with permission. Copyright 2012, American Chemical Society. (B) Schematic diagram illustrating the fabrication of Si wire arrays using a combination of lithography and catalytic etching [91]. Reproduced with permission. Copyright 2011, American Chemical Society. (C) TEM image of GAA strained-Si n-MOSFET [92]. Reproduced with permission. Copyright 2009, IEEE. (D) Schematic diagram of the NIL-IPT workflow [93]. Reproduced with permission. Copyright 2017, IOP Publishing Ltd. (E) Schematic diagram of the microtubule template synthesis. Reproduced with permission [94]. Copyright 2003, Chemistry of Materials. (F) The left inset represents schematics, whereas the middle and right insets are corresponding top view and cross-sectional scanning electron microscopy (SEM) images [95]. Reproduced with permission. Copyright 2014, Macmillan Publishers Limited. (G) Schematic view of the preparation procedure for nanowire arrays [96]. Reproduced with permission. Copyright 2000, Kluwer Academic Publishers.

metallic nanowires is better, which guarantees that the nanowires possess excellent mechanical properties and electronic properties. Besides, Forrer et al. [96] used the anodization of aluminum to fabricate nanoporous alumina as templates for fabricating nanowire arrays. After the deposition of gold into the pores of the alumina, a 15 μm gold layer is deposited as the substrate of the nanowire array. Subsequently, the aluminum base is removed and an array of gold nanowires has been fabricated (Figure 2G).

2.2 | Bottom–Up Methods

Unlike top–down methods, bottom–up methods are involving an additive fashion to prepare nanowires. Among different bottom–up methods, VLS is the most common and most famous fabrication method to prepare semiconductor nanowires. The VLS processing involves four steps. Initially, the alloy catalyst is transformed into droplets either by elevating the temperature or through plasma involvement. Following this, silane (SiH_4) gas is introduced as a precursor. This gas is absorbed by the catalyst droplets to create a supersaturated state, which also serves to inhibit oxidation. Finally, the bottom solid–liquid interface starts to emerge the nucleation and precipitation and SiNWs begin to grow vertically. However, the vertical nanowires are unsuitable for application in a planar device. Therefore, the lateral growth of nanowires is also of great importance. Compared to vertical growth, changing the orientation of the substrate may make a difference. The seed particle starts to move on the substrate laterally instead of growing vertically in the <111> directions and forms a semiconductor nanowire on the substrate (Figure 3A) which is called selective lateral nanoepitaxy (SLE) [103]. Zhang et al. [99] employed the SLE techniques to fabricate lateral InAs nanowires on the GaAs (100) semi-insulating substrates which use colloidal Au nanoparticles as catalysts. In this work, it is notable that because of their high aspect ratio, nanowires can accommodate more strain caused by the lattice mismatch than standard thin films. Therefore, the SLE has a wonderful future of heterogeneous device integration. Besides utilizing SLE to fabricate lateral nanowires, nanochannels may also work as the orientation of the substrate in SLE, restricting the growth direction of nanowires. Because of the crystalline nature, nanowires grow unidirectionally and follow a specific crystallographic orientation once the growth starts. Therefore, controlling the initial growth orientation is enough for fabricating the lateral nanowires. Shan et al. [100] have used EBL to form gold nanostrips on the substrate with a diameter ranging from 80 to 150 nm. Subsequently, they deposited a SiO_2 capping strip layer and then involved solution etching to remove the exposed Au strips and preserved a short Au segment as the seeds for VLS growth of SiNWs. Finally, under the control of nanochannels, the SiNWs grew straight out of the channels (Figure 3C). The nanochannel-guided method enables a growth-in-place deployment of nanowires, which owns a great potential to integrate nanowires into the planer device specifically such as the nanowire field effect transistors (NW-FET). However, the nanochannel needs to be designed by EBL, so the diameter of nanowires is limited by the resolution of the EBL; besides, the aforementioned problems of lithography such as high expensive and low wafer throughput also limit the application in mass production.

In fact, the VLS method always involves gas as a precursor to promote the growth of nanowires, which is typically applied

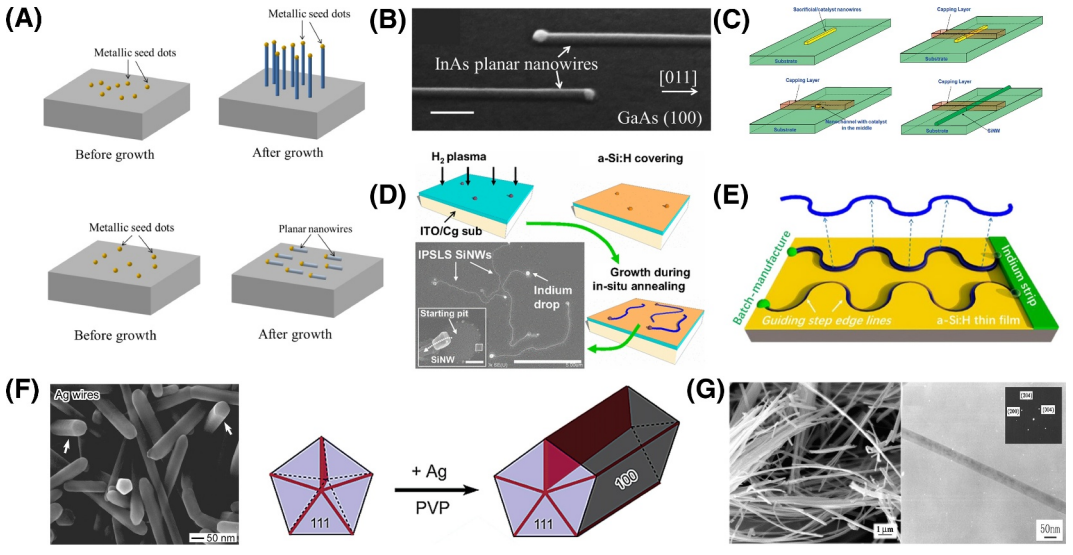

FIGURE 3 | (A) Schematic diagrams illustrating VLS nanowire growth [99]. Reproduced with permission. Copyright 2017, IOP Publishing Ltd. (B) SEM image of two as-grown InAs planar nanowires on GaAs (100) [99]. Reproduced with permission. Copyright 2015, IEEE. (C) Process flow for the fabrication of "grow-in-place" SiNWs using a guiding nanochannel template [100]. Reproduced with permission. Copyright 2008, American Chemical Society. (D) The top three insets are schematic illustrations of the fabrication steps of the IPSLS SiNWs and the bottom inset is the SEM image of typical SiNWs [71]. Reproduced with permission. Copyright 2010, The American Physical Society. (E) The schematic of fabrication of the nano-spring [74]. Reproduced with permission. Copyright 2017, American Chemical Society. (F) The left inset is the SEM image of silver nanowires and the right inset is the schematic illustration of the morphology process in fabricating AgNWs [101]. Reproduced with permission. Copyright 2003, American Chemical Society. (G) The left inset is the typical SEM image of anatase TiO_2 nanowires and the right inset is a TEM image of a single anatase TiO_2 nanowire [102]. Reproduced with permission. Copyright 2002, Elsevier Science B.V.

from the top of catalyst droplets and encourages a vertical growth of nanowires naturally [104]. Instead, a-Si thin film deposited on the substrate taken to replace the gas precursor will form an energetically favorable bottom interface between the catalyst droplets and the substrate, which can help lead catalyst droplets to proceed in-plane. This IPSLS mechanism was first proposed by Yu et al. [71] in 2009. As Figure 3D demonstrates, under the hydrogen plasma treatment, indium (In) with a low melting point melts into droplets, functioning as the catalyst. Then by introducing silane plasma, an a-Si coating is deposited on the substrates at a low temperature, which prevents the catalyst from melting and the happening of VLS growth. Subsequently, the substrate is heated and the catalyst melts again and begins to absorb the nearby a-Si as a precursor to establish a supersaturation state. Simultaneously, the crystalline silicon (c-Si) seeds emerge at the bottom, located between the droplet and the substrate. As the silicon seeds reach the critical size, the catalyst droplets move against the biggest nucleation and SiNWs continue to grow along the substrate laterally (Figure 3D). Apart from the difference in the lateral growth and vertical growth of nanowires, the morphology of nanowires is also an important factor that would influence the performance of flexible sensors. Fortunately, it is easy to design the line shape of nanowires by forming a step edge on the substrates, which just needs a low-resolution standard lithography [74]. The a-Si is coated on the sidewalls of step edges and forms an extra absorption interface for the catalyst droplets, which can attract and lead the droplets to move along the step edge (Figure 3E). By changing the patterns of the lithography, it is easy to fabricate in-plane nanowires with differently designed morphologies. Different from the above nanochannel-guided method, this step-edge-guided method is more economical because the low-resolution lithography is just enough and provides flexibility to edit the morphology of nanowires. Notably, the key difference between the IPSLS method and the VLS method lies in the phase of the precursor material. In the IPSLS method, the precursor transitions from solid a-Si to liquid within the catalyst droplet, enabling continuous absorption of silicon atoms from the substrate surface. This contrasts with the VLS method, where silicon atoms are absorbed from gaseous silane. The concentration of silicon atoms in solid a-Si is much higher than in gaseous silane, leading to a significantly faster growth rate in the IPSLS method—potentially over a hundred times faster under optimal conditions.

With respect to the fabrication of metallic nanowires, the polyol process is one of the primary strategies because of its ideal control over morphology, high yield, low reaction temperature, and so on [105, 106]. The core principle of the polyol process is that when the solution temperature increases, the polyol solvent gradually reduces metal ions to metal, which first nucleate to form seeds and finally grow into nanowires. Sun et al. [101] successfully fabricated AgNWs with a diameter ranging from 30 to 40 nm and a length of up to 50 μm (Figure 3F). In this work, ethylene glycol is used as both the reducing agent and solvent for its high boiling point and proper viscosity, and polyvinylpyrrolidone is used as the capping agent, which both protects the nanowires from aggregating into bundles and promotes the anisotropic growth of AgNWs. Besides, different from the polyol process, hydrothermal synthesis is also widely used for its low cost, low temperature, high yield, and scalable process. Zhang et al. [102] used the hydrothermal process for fabricating TiO_2 nanowires, which have high crystallinity with diameters ranging from 30 to 45 nm (Figure 3G). Besides, the synthesis process is simple but produces large amounts of single-crystalline nanowires at low cost and high purity.

Top–down methods involve subtractive processes on materials, primarily relying on lithographic techniques to achieve high-precision positional nanowire etching. These methods require sophisticated equipment and are limited by advancements in lithographic techniques, resulting in low throughput, reduced production efficiency, and high costs for nanowire fabrication. In contrast, bottom–up methods use additive processes to guide the synthesis of nanowires from individual silicon atoms. The classical VLS method involves the catalyst absorbing silicon atoms from silane to guide nanowire growth. The IPSLS method combines low-resolution lithography with catalysts to achieve morphology-variable nanowire growth. Bottom–up methods are cost-effective and highly efficient, making them suitable for large-scale production. However, they may not match lithographic techniques in ensuring uniformity and precise positioning of nanowires.

To advance the application of nanowires in flexible sensors, it is crucial to combine the advantages of both top–down and bottom–up methods, developing techniques that offer high precision alongside large-scale production capabilities.

2.3 | Transfer and Assembly Methods

Nanowire-based flexible sensors always consist of flexible substrates and active components such as nanowires. However, single-crystalline semiconductor nanowires are always fabricated by VLS, IPSLS, or similar techniques, which induce a relatively high-temperature environment, causing most flexible substrates to shrink or degrade [107, 108]. In comparison, a-Si can be deposited at a low-temperature environment by vacuum deposition techniques, but has a bad mobility compared to c-Si. Besides, the organic semiconductor can also be fabricated in a room-temperature environment by solution-based processing. Similarly, the inherently bad electronic properties limit their application. Therefore, transferring and assembling c-Si nanowires from hard substrates to soft substrates is a promising method in the application of fabricating nanowire-based flexible sensors [109], which separates the high-temperature synthesis of nanowires from the low-temperature assembly of flexible sensors (Figure 4A). Lee et al. [110] used a contact-printing method to transfer c-Si nanowires or devices from the donor substrate to flexible substrates such as polydimethylsiloxane (PDMS). In this work, they categorize their contact-printing techniques into three methods such as single-transfer printing, double-transfer printing, and multiple-transfer printing (Figure 4B). Although the number of transfers and the order of device assembly are different, the core principle involves adhesive receiver substrates to peel off nanowires or nanowire devices from the donor substrates. This contact-printing method is simple to operate and broadens the application of nanowire devices on different substrates, but also faces critical issues waiting to be addressed such as bad metal contact quality, low

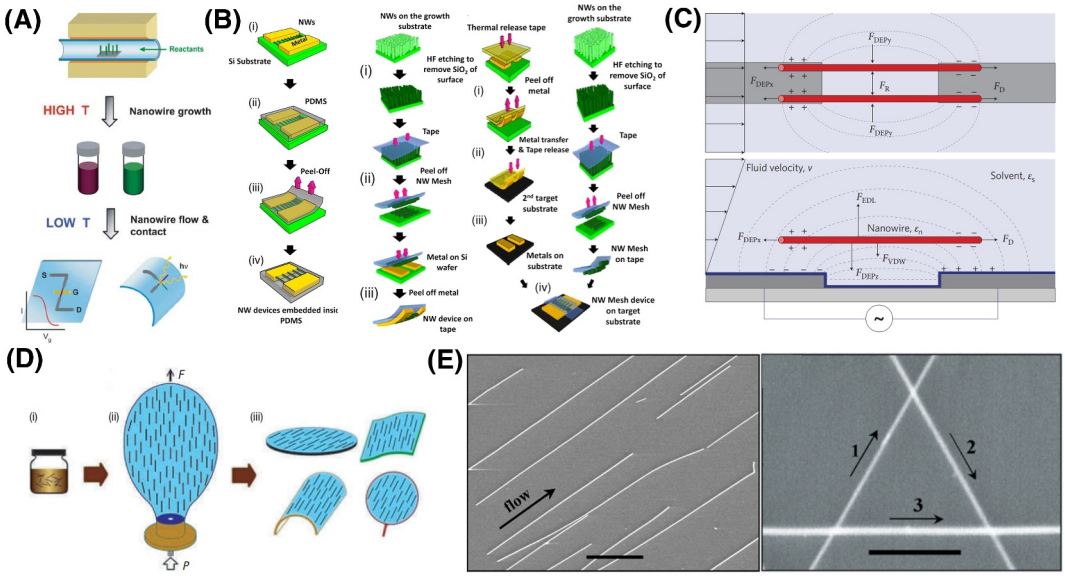

FIGURE 4 | (A) Nanowire growth and device assembly on glass and plastic substrates [109]. Reproduced with permission. Copyright 2005, IEEE. (B) Schematic diagrams of contact-transferring methods of transferring nanowire devices onto PDMS [110]. Reproduced with permission. Copyright 2010, National Academy of Sciences. (C) Illustration of the dielectrophoretic assembly process [111]. Reproduced with permission. Copyright 2010, Macmillan Publishers Limited. (D) Illustration of transferring nanowires from the solution to polymer bubble film by BBF process [112]. Reproduced with permission. Copyright 2007, Nature Publishing Group. (E) The left inset is the SEM image of parallel arrays of InP nanowires aligned by channel flow and the right inset is the SEM image of an equilateral triangle of GaP nanowires [113]. Reproduced with permission. Copyright 2001, The American Association for the Advancement of Science.

device yield and lack of control over the orientation of nanowires.

Therefore, to solve the above problems, a method which can precisely control the alignment of nanowires is needed. In 2010, Freer et al. [111] proposed a self-limiting single-nanowire assembly method. Their team used a low aspect ratio channel (0.013) to obtain a uniform horizontal flow, which is a core factor of high deposition yields of nanowires on electrodes, because the uniform horizontal flow provides a stable force to sustain the nanowires in suspension. Simultaneously, within a distance nanowires would polarize under the influence of the AC electric field generated by the patterned electrodes and can be attracted to the electrodes by the dielectrophoretic forces. In this assembly process, dielectrophoretic, hydrodynamic, and electrostatic double-layer interactions reach a relative balance and enable precise control over the placement of nanowires (Figure 4C). Compared to other assembly methods, their team achieved 98.5% single nanowire yield on 16,000 electrode sites and enabled low defect assembly and precise control. However, the generation and precise control of the uniform horizontal flow and the ability to reproduce uniform process conditions limit the application. Figure 4D shows a novel method to transfer nanowires by bubble films. In this work, Yu et al. [112] first prepared a homogeneous polymer suspension of nanowires with a controlled concentration. Subsequently, they used a circular die to expand the polymer suspension into a bubble. During the expansion process, the shear stress adjusts the orientation of nanowires as the bubble expands in the vertical direction. Therefore, the separation of nanowires remains uniform and the angular deviation can be less than 10°. Finally, after transferring the bubble film to substrates or other surfaces, the blown bubble film (BBF) process is completed. This BBF process provides a novel method to achieve large-area uniformly aligned and controlled-density transferring of nanowires and can be applied on both rigid substrates, flexible substrates, and even highly curved surfaces. Although the density of nanowires is limited, the BBF process now is mainly suitable for areas such as biological/chemical sensors and displays. Besides, Huang et al. [113] reported an approach for the hierarchical assembly of nanowires. The method used the shear forces produced by fluid flows to control the alignment and separation of nanowires. As the flow rate increased from 4 to 10 mm/s, the width of angular distribution decreased rapidly at the beginning and finally reached a constant value. In addition, using different flow directions for sequential steps, complex crossed nanowire networks can be prepared by a layer-by-layer assembly such as an equilateral triangle (Figure 4E). This fluidic assembly method demonstrated the possibility of alignment of nanowires with control of the average separation and the width of angular distribution and layer-by-layer assembly of crossed and more complex structures.

3 | Applications in Wearable Electronics

Real-time biometric monitoring, including activity tracking, respiratory monitoring, sleep monitoring, heart rate monitoring, blood pressure monitoring, and the detection of other signals carrying biometric information, has gained increasing importance over the past few decades with advancements in medical technology. Compared to traditional bulky, expensive monitoring equipment, wearable electronics undoubtedly offer a compact, portable, low-cost, and low-power alternative that is conducive to long-term wear for continuous signal detection

[114–116]. Additionally, the applications of wearable electronics extend beyond merely collecting signals from the body; sensors, acting as a third "electronic eye" for humans, receive external signals such as pressure, temperature, and humidity, and perform quantification and display, enhancing or compensating for people's perception of these external signals. Furthermore, the field of wearable electronics also focuses on achieving capabilities that surpass human sensory abilities, such as electromagnetic shielding, flexible displays, chemical gas detection, and more. These functions can be realized and even integrated into wearable electronics, enabling the collection of signals not only from within the body but also from the body's surface and its surroundings. Wearable electronics are considered one of the key areas for future sensor development, with promising application and development prospects.

3.1 | Health Monitoring

With the outbreak of Coronavirus disease 2019, the virus detection technique is gaining greater significance. RT-PCR is a typical technique to detect viruses which reverse transcribes RNA to form template cDNA and amplify to synthesize the target fragment in order to achieve the function of virus detection. However, this technique needs sample collection, a relatively long process time, and bulky instruments. The time required for this detection process may exacerbate the spread of the virus, which seriously threatens people's lives. Therefore, on-site virus detection is of great importance. This technique should be flexible and portable enough to meet the needs of wearable electronics, low cost for mass fabrication, and fast response time, which guarantees the timely detection of viruses. As shown in Figure 5A, Xue et al. [117] proposed an intelligent face mask, which enables on-site virus detection. This intelligent face mask consists of three layers. The outside polycarbonate porous membrane layer collects droplets and protects sensors. The middle layer is the core of the face mask, which functions as the sensitive layer composed of the nanowire array, and the bottom supporting layer is made of a flexible polyethylene terephthalate substrate to adapt to curved surfaces. In this work, the nanowire array is parallel-patterned on the substrates with a spacing of 75 nm, which helps capture the target spike protein and ensures the device's repeatability. As the target antigens are adsorbed on the nanowires and bind to antibodies, the impedance measured also increases. By this impedance model, the intelligent face mask can collect the exhaled viral aerosols within several minutes and send warnings to the smartphone. Besides, this technique also has a nice mechanical performance and can function normally under slight bending (< 15°).

UV is also considered one of the important factors affecting human health. Moderate UV exposure can help synthesize vitamin D and enhance the level of a beta-endorphin molecule, which can improve our moods. However, too much UV exposure also causes damage to our bodies. High-intensity UV radiation can damage people's eyes, lead to skin burns, and cause irreversible damage to DNA, which may cause cancer or lead to

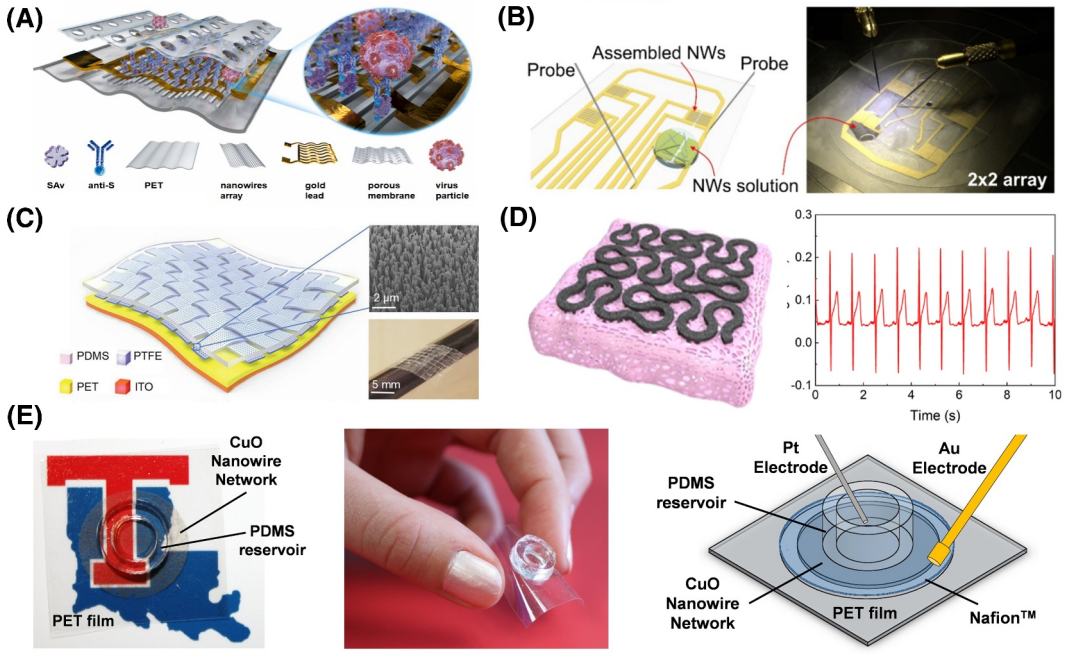

FIGURE 5 | (A) Schematic illustration of the nanoscale sensor design [117]. Reproduced with permission. Copyright 2021, Elsevier B.V. (B) The left inset is the assembly of ZnO nanowires and the right inset is an image of ZnO nanowires assembled by dielectrophoresis between Au electrodes [118]. Reproduced with permission. Copyright 2018, IEEE. (C) Schematic illustration of the flexible weaving constructed self-powered pressure sensor [119]. Reproduced with permission. Copyright 2018, WILEY-VCH Verlag GmbH & Co. KGaA, Weinheim. (D) The left inset is the schematic of the AgPHPUS and the right inset is ECG signals measured instantly with AgPHPUS electrodes [120]. Reproduced with permission. Copyright 2021, Springer Nature. (E) The left inset is a top down photograph of an assembled sensor, the middle inset is a demonstration of device flexibility, and the right inset is an annotated illustration of the glucose sensing experimental setup [121]. Reproduced with permission. Copyright 2017, IOP Publishing Ltd.

immune system damage. In 2018, Nunez et al. [118] proposed a wearable dosimetry to monitor the intensity of UV. They involved zinc oxide (ZnO) nanowires as photoconductors of sensors. Because of the wide energy band gap of ZnO (E_g = 3.3 eV), it has low absorption of visible light but strong absorption of UV with high selectivity and sensitivity. Bulk ZnO has a slow optical response and bad mechanical properties, and this hinders its application in the field of wearable electronics. Therefore, their team employed ZnO nanowires in order to overcome the problems of the slow optical response and be in conformal contact with the body. Firstly, they grew ZnO nanowires using VLS mechanisms and then transferred them in a solution. Subsequently, they assembled them onto large-area flexible substrates to form 4 × 4 arrays of UV photodetectors, which showed a high sensitivity with high Iphoto/Idark ratios above 1000% and fast response time (t_r ~ 12 s). Besides, the dark current was also measured under a bending radius from 5 to 27 mm and was affected slightly but functioned normally.

The heart, as the energy pump of human daily lives, takes a leading role in the human body, and the pulse wave is an important signal that contains a lot of information and helps prevent cardiovascular disease. Conventional methods are the cuff type and have a complex structure and poor portability, which are unsuitable for long-term and dynamic monitoring. Therefore, a non-invasive, portable, and user-friendly pulse wave sensor has a promising future. As shown in Figure 5C, Meng et al. [119] proposed a weaving-constructed self-powered pressure sensor (WCSPS), which can measure the pulse wave velocity and blood pressure for the long term. The WCSPS is composed of four layers. The bottom layer is made of ITO as the back electrode, and the upper layer is an electrification layer with polyethylene terephthalate (PET). Subsequently, an interlaced woven structure of polytetrafluoroethylene (PTFE) strips acts as another electrification layer and the top layer is a PDMS layer protecting the PTFE strips. Specifically, their team used a plasma etching technique to form vertically aligned polymer nanowires connecting PTFE to PET. On the one hand, these nanowires help form contact between PET and PTFE more intimately and enhance the conductivity. On the other hand, they improve the surface triboelectrification and the electrical signal output. Simultaneously, the high aspect ratio of nanowires means they can deform easily and have a wonderful sensitivity to detect subtle pressure. It was verified that the introduction of nanowires increased the sensitivity of pressure sensing by 1.4 times. In this work, the WCSPS demonstrates an excellent sensitivity of 45.7 mV Pa^{-1}, a fast response time of less than 5 ms, and excellent mechanical properties, functioning normally after 40,000 cycles of continuous operation. Besides, from employing pressure sensors to monitor heartbeat and blood pressure, monitoring the electrocardiogram (ECG) is a more direct method. The electrode in the ECG system takes a leading role in capturing and transmitting signals. Conventional methods are using silver/silver chloride (Ag/AgCl) to fabricate wet electrodes. Despite the high conductivity and stable contact between electrodes and the skin, the wet electrodes may gradually dehydrate, leading to an impedance increase and irritating the skin which can bring users discomfort. In 2021, Huang et al. [120] proposed a flexible silver nanowire dry electrode. They employed hydrophilic polyurethane (PU) sponge, AgNWs, and polyvinyl butyral (PVB) to fabricate fractal curve sponge with high conductivity and nice mechanical properties. After 1200 cycles with 1 mm compression, the resistance of the electrodes changed by < 4%. Under the compression of 5 mm, the resistance only changed by ~20%. Additionally, the electrodes demonstrated a stable electrical property whose conduction characteristic was still linear after 1200 cycles of cyclic voltammetry and showed an accurate record of ECG, which can be comparable to commercial Ag/AgCl electrodes. This work used the excellent electric and mechanical properties to fabricate a flexible, biocompatible, and stretchable dry ECG electrode that guarantees long-term ECG monitoring (Figure 5D).

In recent years, diabetes has become increasingly common worldwide and has become a serious safety hazard to human health. Glucose monitoring sensors make up a large market, but conventional glucose sensors rely on an enzymatic electrochemical sensing mechanism. The inherent nature of enzymatic sensors indicates that they always have an excellent selectivity but bad stability, which represents that they are not suitable for long-term monitoring. In order to solve the above problems, attention is being paid to nonenzymatic glucose sensors. Among them, copper (Cu) and its oxides are considered as promising candidates for their high abundance, low cost, and chemical and physical stability. Bell et al. [121] fabricated a flexible, transparent, and nonenzymatic CuO nanowire glucose sensor. They first used a thermal oxidation process to grow CuO nanowires on the Cu microparticles with a diameter of about 35 nm and a length of about 5.2 μm. Then, they transferred the nanowires onto PET at a specific pressure and temperature and finally developed the glucose sensor (Figure 5E). CuO nanowires have a strong ability to catalyze glucose oxidation to form a current, which is the core principle of this sensor. Additionally, these glucose sensors can detect small solution volumes of 2 μL and a physiologically relevant range of glucose levels from 0 to 12 mM glucose. Although the sensitivity of this sensor is relatively low compared to other glucose sensors, it is still within an acceptable range. Besides, this glucose sensor is capable of functioning with external bodily fluids (tears, saliva, etc.) instead of requiring direct access to patient blood, promoting patient usage, comfort, and compliance.

3.2 | Fitness Tracker

The body motion is an important signal which contains much valuable information for insights into the health and fitness of people and also can be applied to the human–machine interface. However, body motion monitoring requires good mechanical properties that allow sensors to bear relatively large bending and stretching, stability, and biocompatibility, guaranteeing that sensors can be worn for long-term use with comfort [122, 123]. Therefore, combining nanowires with textiles to fabricate e-textiles is considered a solution. The advantages of electric properties and mechanical properties of nanowires can compensate for the weaknesses of conventional e-textiles, such as low conductivity, increased elastic modulus of the textiles, and so on. In 2019, Yao et al. [124] proposed a multifunctional electronic textile involving AgNW composites. First, they uniformly coated the glass with AgNW solution. Then, they evaporated the solvent to deposit AgNWs and spin-coated

thermoplastic polyurethane (TPU) solution above the AgNWs and subsequently solidified the TPU as a protective and fixed layer. Finally, AgNW/TPU nanocomposites were transferred from the glass substrate to the fabric using a heat-press method at 140°C and the e-textiles were successfully fabricated. By designing a sandwich structure in which the top and bottom layers were made of AgNW/TPU electrodes and the middle layer was composed of Ecoflex as the dielectric, they achieved a capacitive strain sensor for precisely monitoring body motion for the long term (Figure 6A). They reported that the capacitance change is linearly proportional to the joint bending angle and has a large range of loading and unloading to 50%. Simultaneously, after 500 cycles of loading and unloading, the gauge factor of the strain sensor changed within 0.02, which demonstrated a nice stability. Besides, from using nanowires as electrodes to form a capacitor for body motion monitoring, the piezoresistive characteristics of nanowires can also be employed. As shown in Figure 6B, Shin et al. [125] invented a sandwich structure sensor using two different types of nanowires. They used the piezoresistive properties and conductivity of AgNWs as electrodes for detecting the motions and the piezoelectric properties of ZnO nanowires for sensing instantaneous dynamic motions. The top layer and the bottom layer consisted of PDMS and AgNWs serving as sensitive layers and electrodes of the middle ZnO nanowires layer. As the device was stretching or bending, the AgNW network also elongated which increased the resistance of the entire system. At the bending angle of 70°, the resistance of the AgNW electrode increased to ~2000%. Besides, as the device was deformed by external forces, the ZnO layer released bound charges, which were collected by the top and bottom AgNW electrode and generate piezoelectric voltage. For example, when the bending speed ranged from 65 to 75 mm/s, the output voltage increased from 0.97 to 1.48 V. Specifically, the piezoelectric voltage had a polarity that reversed when the bending direction was changed. The integration of the AgNW layer and ZnO nanowires layer provided both motion information and instantaneous motion detection.

Sleep is one of the most important physiological activities of humans, but in recent years many people have suffered a sleep disorder. More and more attention is being paid to sleep quality. All kinds of sleep monitoring sensors are proposed to try to solve the problem. However, the information about sleep is always multifaceted, such as snoring, tooth grinding, breathing, turning over, and so on. These important signals are often ignored by current popular flexible solutions that record hand-

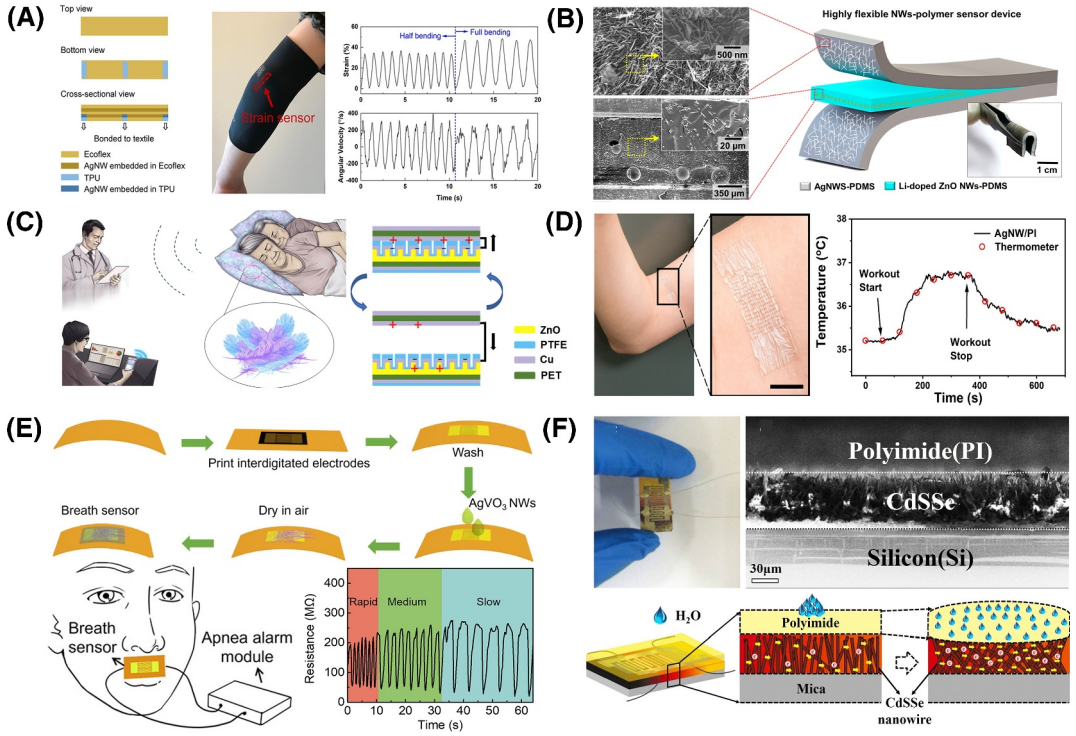

FIGURE 6 | (A) The left inset is a schematic of the textile-integrated capacitive strain sensor, the middle inset is a photo of the placement of the textile patch, and the right inset is strain and angular velocity as functions of time [124]. Reproduced with permission. Copyright 2019, American Chemical Society. (B) Schematic representation of the sensor device consisting of two main parts: resistive and piezoelectric sensing elements [125]. Reproduced with permission. Copyright 2017, American Chemical Society. (C) The left inset is a schematic illustration of a pillow filled with flexible self-powered triboelectric sensors and the right inset is the working mechanism of the sensor [126]. Reproduced with permission. Copyright 2020, Elsevier Ltd. (D) The left inset is that the AgNW/PI temperature sensor is attached to the skin near the biceps and the right inset is temperature recorded [127]. Reproduced with permission. Copyright 2019, American Chemical Society. (E) The top inset is the fabrication of the breath sensor, the left inset is a schematic diagram, and the right inset is a real-time monitoring of breath at various breathing rates [128]. Reproduced with permission. Copyright 2023, American Chemical Society. (F) The top inset is a real image of the as-prepared sweat sensor and an SEM image of the sensor, and the bottom inset is the schematically theoretical diagram of humidity sensing of the sensor [129]. Reproduced under terms of the CC-BY license. Copyright 2019, The Authors, published by Springer Nature.

related locomotor activities to infer the sleep data. Therefore, Zhang et al. [126] presented a fractal down-like structure sleep monitoring sensor. They first grew ZnO nanowire arrays on the fractal PET slice and then deposited a Cu layer and a PTFE layer on the fractal structure substrate in turn. By this means they fabricated the Cu electrode and the PTFE electrode as the core component of this triboelectric sensor (Figure 6C). When external force was applied to the sensor, the contact area between the two electrodes increased. Because of the difference in electron affinity of the two different materials, the process would lead to an interfacial charge separation and generate a triboelectric voltage. Additionally, the nanowire arrays on microelectrode branches effectively increased the efficiency of the triboelectric effect by enhancing the roughness of substrates. This sensor can be filled into the conventional bedding pillow, which guarantees a comfortable experience and realizes a remote and imperceptible monitoring of sleep.

Many disease symptoms are reflected through body temperature. Body temperature can also be used as an important physiological indicator for complex analysis of physical conditions. Long-term monitoring of temperature needs a flexible sensor to be attached to the body surface closely in order to get the most accurate temperature. Meanwhile, the temperature sensor should be vapor-permeable, lightweight, and stretchable to bring the wearer a comfortable experience to ensure long-term wear. AgNWs are found to have wonderful mechanical properties but also a good temperature coefficient of resistance (TCR), which is higher than the bulk Ag. However, the resistance of AgNWs is also influenced by the applied strain, which may affect the measurement of body temperature. Cui's team [127] proposed a solution to this problem. They fabricated a Kirigami-inspired structure sensor. This special structure allowed the resistance of the temperature sensor to slightly change under a large strain. When the sensor was stretched to 100% strain, the change of resistance was within 0.05%. Besides, with a small thickness of 9 μm, the temperature sensor could be conformally attached to the skin and provide accurate temperature monitoring. The TCR was influenced by the densities of AgNWs and the annealing temperature. With a density of 2.053/μm^2 and an annealing temperature of 200°C, the TCR of the temperature sensor was about 3.32×10^{-3}/°C and the sensitivity of 0.47 Ω/°C. After 1000 cycles of cyclic tensile testing at 100% strain, the resistance of sensors remained stable (Figure 6D).

Breath plays an important role in the diagnosis of cardiovascular diseases and the treatment of sleep apnea. The time and rate of breath can be used to analyze the health condition of people and send warnings on time. The conventional clinical process incorporates a face mask to cover the nose and mouth of the user completely, and this system is connected to a bulky machine. This method is inconvenient and expensive, which limits the wide application for long-term monitoring and a comfortable experience. Therefore, instead of monitoring airflow directly, the water vapor content in exhaled breath can also be used to characterize respiratory conditions to fabricate portable low-cost breath sensors. As shown in Figure 6E, Yan et al. [128] proposed a long-term, ambulatory breathing monitoring sensor based on $AgVO_3$ nanowires. The $AgVO_3$ nanowires were synthesized using a hydrothermal method as large surface-to-volume active semiconductors. Subsequently, they used drop-casting to transfer $AgVO_3$ nanowires to the flexible polyimide (PI) substrates. As the water vapor was absorbed by sensors, it acted as an electron-donating gas on semiconductive oxides, which led to a decrease in resistance. By detecting the change of resistance of sensors, we can realize the monitoring of breath. This sensor can detect a large range of relative humidity from 20% to 90% and has a fast response time of 0.6 s and recovery time within 1.2 s, which is enough to detect human breath with different breathing rates. By using this sensor, long-term, comfortable, dynamic breath monitoring can be realized to diagnose respiratory diseases and detect special conditions such as cardiac arrest to provide first aid. The humidity sensor can also be applied to another important factor, sweat. As one of the easiest accessible bodily fluids, sweat contains much physiological information, which can be used for the different stages of dehydration. Zhang et al. [129] proposed a wearable sweat monitoring sensor involving CdSSe nanowires. Comparable to the above breath-monitoring sensor, this sweat sensor used the piezoresistive property to measure relative humidity. CdSSe nanowires show great stress sensitivity. As the moisture-sensitive PI layer swells when exposed to water, it will generate hygroscopic expansion applied to the CdSSe nanowires layer, whose resistance would decrease linearly (Figure 6F). Besides, the concentration of salt in sweat also influenced the resistance of this sensor. With the increase in salt content, the current reduces linearly. These properties enable moisture and salt detection for long-term wearable sweat monitoring and provide real-time feedback on the user's fitness condition and stages of dehydration. Besides, a short summary of nanowire-based wearable electronics is presented in Table 2.

Nanowires are recognized as an ideal component for emerging flexible sensors because of their remarkable mechanical properties and unique sensing capabilities. They are commonly integrated with flexible substrates to achieve superior sensor performance. The impact of the interfacial binding forces significantly affects the performance of flexible sensors, especially concerning the stripping strength of the nanowires relative to the substrate.

For stress-sensitive sensors, the matrix acts as a medium through which forces from the substrate are transferred to the nanowires. As external stress increases, the interfacial binding forces also increase until they reach a critical point where failure occurs, either by fracture or slippage at the interface. When these forces exceed the stripping strength [136, 137], the effective transmission of stress is compromised, leading to decreased sensitivity and hysteresis in the sensor's response curve.

In contrast, for nonstress-dependent sensors, the interfacial binding force primarily impacts the robustness and durability of the device. For example, nanowires embedded in a matrix experience greater strains than those suspended freely, which can lead to earlier failure under lower applied forces [138, 139].

Notably, when the interfacial forces reach debonding strength, the slippage of nanowires is often reversible within certain limits, meaning that applying stress within a defined range minimally impacts sensor performance. Although there have been studies on measuring and modeling nanowires and interfacial forces, systematic analysis of how nanowire sliding

TABLE 2 | Typical nanowire-based wearable electronics reported recently.

Materials	Fabrication strategies	Function	Substrate	Mechanical properties	References
AgNWs	Polyalcohol reduction	ECG monitoring	Hydrophilic polyurethane sponge	1200 cycles with 1 mm compression	[120]
AgNWs	Polyol reduction	Motion monitoring	Textile	500 cycles of loading and unloading	[124]
AgNWs	Polyol method	Temperature sensor	PI	Stretch under 100% strain	[127]
CuNWs	Hydrothermal	Strain sensor	Polymer	Strain up to 185% twisting angle of 180° and 270° after 500 cycles	[130]
AuNWs	Wet chemical method	Health monitoring	Fabric	Strain up to 73%	[131]
Polymer nanowires	Nanoscale soft printing	Virus detection	PET	Bended (< 15°)	[117]
Polymer nanowires	Plasma-etched	Blood pressure sensor	PDMS/PET/ITO	Over 40,000 cycles' continuous operation	[119]
Polymer nanowires	—	Temperature sensor	PDMS	Bending radius of 7.5 mm	[132]
SiNWs	VLS	Strain sensor	PDMS	Strain (> 45%) and durability (> 10,000 cycles)	[133]
SiNWs	Thermal evaporation	Food inspection	—	Repeatedly bent to large angles (~160°)	[134]
SiNWs	IPSLS	Strain sensor	PDMS	A high stretchability of > 40%	[79]
SiNWs	VLS	Airflow detection	PET	—	[135]
CuO nanowires	Thermal oxidation	Glucose sensor	PET	—	[121]
ZnO nanowires	VLS	UV photodetector	Polyvinyl chloride	Bending radius of 5 mm	[118]
ZnO nanowires and AgNWs	—	Motion and temperature sensor	PDMS	Bending angles of 90° and stretching distances of 4 mm	[125]
ZnO nanowires	Hydrothermal	Sleep monitoring	PET	—	[126]
CdSSe nanowires	CVD	Sweat sensor	Mica	—	[129]
$AgVO_3$ nanowires	Hydrothermal	Breath sensor	PI	—	[128]

specifically influences performance remains relatively limited. To address this gap and develop superior flexible sensors, it is necessary to explore relevant theoretical guidance and research directions.

4 | Applications in Brain–Computer Interfaces

The brain, as the most central and enigmatic organ of the human body, has long been the focus of efforts to unravel its mysteries regarding how it functions and how thoughts are generated, questions for which there is still no mature and systematic explanation. BCIs, as technologies capable of real-time monitoring of brain signals, are considered one of the closest approaches to answering these questions [140]. The development of computer technology and signal processing techniques has also made it possible to interpret EEGs. By monitoring brain signals through BCIs and translating them into corresponding languages, high-efficiency communication and low-latency control, among other "future" technologies, can be achieved. For patients with traumatic brain injuries, BCIs can assist in conveying their thoughts, thereby transcending physical constraints [141, 142]. BCIs can also achieve stimulation of specific neurons as a therapeutic approach for brain disorders such as epilepsy [143, 144]. When combined with optogenetics, BCIs can modulate neuronal activity, thus controlling the switch of cellular and animal behaviors.

BCI technology facilitates the connection between the brain and the external environment, playing a critical role in external control and medical diagnostics. BCIs can be classified into invasive and non-invasive types based on their operational principles.

1. Invasive BCIs: Invasive BCIs typically use probes inserted into brain tissue to directly read intracranial electrophysiological signals, which are then processed using machine learning techniques to extract relevant frequency bands for translation. However, implantable electrodes can cause damage to brain tissue, leading to inflammatory responses and gliosis, thereby limiting long-term monitoring. Reducing probe size is crucial for minimizing tissue damage and achieving stable long-term monitoring. Compared to commonly used microscale probes, nanowires offer significant advantages. Their nanoscale dimensions minimize tissue injury and provide excellent spatial resolution. Although nanowires exhibit higher impedance than conventional probes, the reduced defect density at the nanoscale results in enhanced electrical conductivity and signal-to-noise ratio. These advantages make nanowires a promising candidate for future invasive BCIs.
2. Non-invasive BCIs: Non-invasive BCIs employ electrodes placed on the scalp to record EEG signals from the cerebral cortex. Based on electrode type, non-invasive BCIs can be categorized into wet, semi-dry, and dry electrodes. Wet electrodes form stable contacts with the skin surface, providing excellent conductivity but requiring regular maintenance because of moisture evaporation, making them unsuitable for long-term monitoring. Additionally, they can irritate the scalp, causing user discomfort during extended wear. Dry electrodes address these issues but face challenges, such as complex and unstable contact with the skin, which can be influenced by factors such as hair. Increasing the conductivity of dry electrodes can effectively reduce contact impedance and improve the signal-to-noise ratio. Nanowires, as an excellent conductive filler, can meet flexibility requirements for tight skin contact while enhancing electrode conductivity. For the development of next-generation portable, high-performance, and long-term monitoring dry electrode BCIs, nanowires' outstanding mechanical and electrical properties position them for broad application.

4.1 | Neural Probes and Electrodes

Neural probes are considered a promising method for potential therapies for neurological and neurodegenerative diseases for their ability to record EEG and stimulate specific regions as treatment. However, the diameter of conventional neuro probes is at the micrometer level. As these neuro probes are implanted into brain tissue, they cause both acute/chronic trauma, leading to inflammation, which induces glial scarring at the injury site, improving the resistivity between the neuro probe and brain tissues and restricting the long-term signal recording. Therefore, reducing the diameter of neuro probes is considered a solution to this problem. Kang et al. [145] fabricated a subcellular single-crystal Au nanowires (AuNWs) neural probe with a diameter of about 100 nm. They used a vapor transport method to grow AuNWs on a c-cut sapphire spatial substrate vertically, which is a high single-crystal. Because of the near-perfect crystallinity, the AuNWs have better conductivity and mechanical property. AuNWs showed a resistivity of $2.08 \times 10^{-8}\,\Omega$m, which is smaller than bulk Au. Specifically, AuNWs demonstrate superior flexibility; they can be bent into a U-shape under pressure and still recover their original shape without fracturing. This unique mechanical property can be attributed to its high aspect ratio and high degree of crystallinity. As the scale decreases, fewer defects result in better stability for nanowires compared to bulk materials. Nanowires demonstrate a robust yield strength of 1.54 GPa, which is 10 times that of bulk materials. These mechanical characteristics enable nanowires to achieve long-term stable monitoring in brain tissue. Besides, as shown in Figure 7A, compared to the tungsten neuro probe, the AuNW neuro probe has a better recording of the EEG with a high signal-to-noise ratio. Moreover, the nanoscale dimensions of nanowire probes facilitate long-term, stable electrical signal monitoring. Compared to traditional probes, nanowires cause significantly reduced inflammatory responses upon implantation. The inflammatory response leads to gliosis, which increases the impedance between the probe and the surrounding tissue, thereby limiting long-term monitoring. Nanowires, however, have a natural advantage in maintaining long-term stable electrical performance because of their minimal tissue interaction and lower propensity for causing an immune response. Apart from mitigating the invasive nature of the implants, the small dimension also allows high spatial resolution, which enables the AuNW neuro probe to record single-neuron activity. Nanowires are not only used as the probe but also employed as a conductive layer to improve the ability of the neuro probes to record EEG. In 2017, Lu et al. [146] proposed a flexible and stretchable nanowire-coated fiber probe. Since the optogenetic modulation of genetically identifiable neuronal populations is of great importance to find the neural pathways related to post-injury recovery. Therefore, they were aiming to fabricate a neuro probe which could realize EEG recording and optical stimulation simultaneously. They first produced a flexible optical fiber by thermal drawing as the core of the probe and then deposited a layer of AgNWs with a diameter of 70 nm uniformly upon the optical fiber as a conductive layer to enable neural recording. Finally, a layer of PDMS was deposited as the outside protection layer which prevents the direct contact between AgNWs and tissues and the surface oxidation (Figure 7B). Because of the nice conductivity and mechanical properties of AgNWs, the AgNWs layer improved the conductivity of the neuro probe and was more resilient to bending and stretching deformation than metallic films. Through the design of core–shell structures, this neuro probe combining the transparency of optical fibers with the electrical conductivity and mechanical properties of nanowires enabled the simultaneous performance of optical stimulation and electrical recording.

Besides the single neuro probe used for EEG recording, an array of nanowire probes is also widely used for their better monitoring stability and lower impedance. Ryu et al. [147] proposed a low-impedance and flexible neural probe array based on ZnO nanowires and the conducting polymer PEDOT (Figure 7C). The naturally high surface-to-volume ratio of nanowires reduced the impedance between the electrode and tissue by expanding the effective surface area and provided a high signal-to-noise ratio. Besides, they chose ZnO as the material of nanowires for its low-temperature synthesis process of 75°C, which is suitable for use with a flexible substrate. Although the structure of nanowires reduced the resistivity of the neuro probes, the conductivity of ZnO nanowires was still low. Thus, a

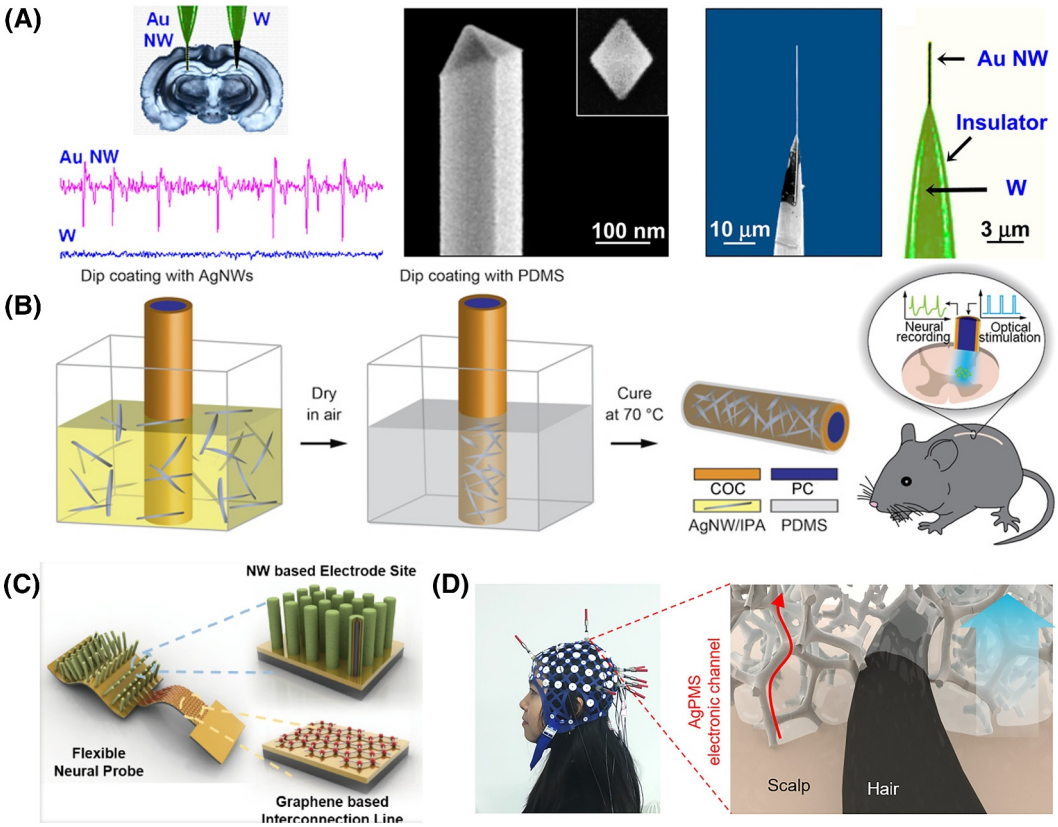

FIGURE 7 | (A) The left inset is a schematic of neural signals using recording electrodes, the middle inset is the SEM image of an AuNW at higher magnification, and the right inset is an SEM image of a combined AuNW-tungsten-tip electrode [145]. Reproduced with permission. Copyright 2014, American Chemical Society. (B) The left inset is an illustration of the fiber probe fabrication and the right inset is a schematic depicting optical stimulation and EEG recording with a fiber probe in a mouse spinal cord [146]. Reproduced under terms of the CC-BY license. Copyright 2017, The Authors, published by The American Association for the Advancement of Science. (C) Schematic diagram of the electrode based on the graphene and nanowire concept [147]. Reproduced with permission. Copyright 2017, American Chemical Society. (D) A photograph and schematic of the contact method of the AgPMS semidry electrode on hairy skin [148]. Reproduced with permission. Copyright 2019, American Chemical Society.

thin-Au film was deposited on the surface of ZnO nanowires in order to increase the probes' electrical conductivity, and subsequently a coating of PEDOT was deposited to provide a porous surface structure, which increased effective surface area and biocompatibility. This core–shell structure neuro probe exhibited a low impedance, large charge storage capacity, and nice biocompatibility, which can efficiently record and monitor the EGG signal and functions of the nervous system or deliver electrical signals to stimulate specific areas of the brain.

As another important development direction for BCIs, the non-invasive EEG electrode has numerous unique advantages over the invasive neuro probe. Firstly, minimizing the damage of BCIs to tissues is urgently needed, but the non-invasive method can avoid this problem completely, which can be applied to clinical human body experiments. Besides, non-invasive BCIs can be easily implemented by attaching the device to the surface instead of requiring surgical implantation of the neuroprobe into the brain. Conductive gel is widely used as the electrode of non-invasive BCIs for its good conductivity and firm contact with the skin. However, gel faces two critical challenges. Over time, the gel gradually dehydrates, and the contact impedance also increases, which limits the long-term monitoring. Additionally, gels mostly irritate the skin and are harmful to hair, which causes discomfort to users. In 2019, Lin et al. [148] presented a flexible, robust, and gel-free EEG electrode hoping to provide a solution to the above problems. They used a vacuum processing step to combine melamine sponges, AgNWs, and polyvinyl butyral together to fabricate a cost-effective AgNWs/PVB/melamine sponge (AgPMS) electrode (Figure 7D). Because of the self-locking structure of AgNWs and the flexible sponge framework, it demonstrated excellent mechanical stability, where even after 10,000 cycles at 10% compression, the conductivity of AgPMS electrodes still remained constant. In order to test the electrodes' chemical stability, they immersed the AgPMS in NaCl solution with different concentrations and found that the resistance of AgPMS increased by 4% for higher concentrations, which demonstrated the stability of the electrode in the presence of a solution such as sweat. Compared to the conventional conductive gel electrodes, the dry AgPMS electrodes can exhibit approximately the same accuracy as that of BCI. Most importantly, owing to the high conductivity and good mechanical properties of AgPMS, this non-invasive BCI electrode can realize a stable long-term EEG recording on hairy skin.

4.2 | Recording, Stimulation and Clinical Application

Because of the high aspect ratio structure, nanowires are considered to possess an excellent mechanical property, which can withstand a certain degree of bending. Additionally, the ballistic transport effect imparted by the wire-like structure gives them better electrical conductivity compared to bulk materials, and they offer superior conductivity over nanoparticle-based nanostructures. Therefore, they are frequently combined with polymers, fibers, and other materials to create flexible materials with good electrical conductivity. As shown in Figure 8A, Sechang Oh et al. [149] utilized AuNWs to fabricate electrodes to record the EEG and electro-oculogram (EOG) for the conductivity and chemical stability. This dry electrode avoided the disadvantages of conductive gels that changed in impedance and led to erroneous or noisy EEG signals. They attached the AuNWs electrode on the forehead of the user, which is the suitable position to sense both EEG and EOG. After signal filtering and processing, they extracted the features of EEG and EOG to control the movement of external robots. The EEG signal was classified into alpha, beta, delta, and theta waves by the entire system. They used these analyses to control the speed of a robot by attention and relaxation levels extracted from EEG signals and the direction of the robot by EOG signals. After experiments, it demonstrated the accuracy rate of the judgment of attention and relaxation is 92.6%.

As the diameter of the nanowire decreases to a few tens of nanometers, which reaches critical biological length scales, nanowire probes such as vertical nanowire electrode arrays show a promising application in intracellular recording. The small scale indicates a low biological damage and high spatial resolution, which can precisely locate and record a single neuron. Besides, the top–down nanowires can be integrated easily with mature complementary metal-oxide-semiconductor technology to realize a mass parallel recording. However, such recording needs a controlled membrane disruption, which leads the measured potential to gradually decrease over time as the membrane reseals. Therefore, Zhang et al. [150] proposed a U-shaped nanowire probe with a point-like FET. They used phospholipid bilayers to modify the kinked NW-FET probes' surfaces, which helped spontaneous insertion through the cell membrane. This spontaneous insertion prevented the measured potential from changing during the recording process and damage to the targeted cell. Besides, the FET structure also enhanced the ability of potential recording, and the quality of intracellular recording of U-shaped nanowire probes was

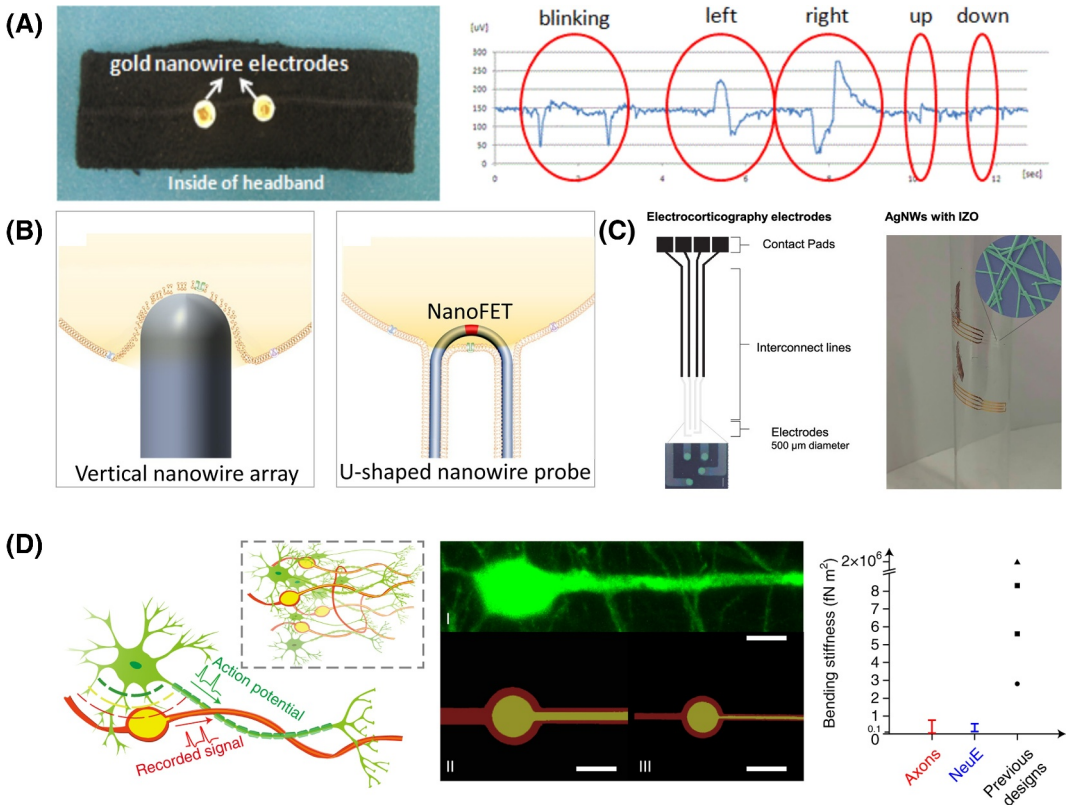

FIGURE 8 | (A) The left inset is the image of the wearable wireless sensing transmitter and the right inset is measured EOG signals with different motions [149]. Reproduced with permission. Copyright 2012, SPIE. (B) The left inset is a schematic of vertical nanowire arrays and the right inset is a schematic of ultrasmall U-shaped nanowire probes [150]. Reproduced with permission. Copyright 2019, Elsevier Ltd. (C) The left inset is the design of the electrocorticography electrode arrays prototype and the right inset is an image of prototypes wrapped around a glass tube demonstrating the device's flexibility [151]. Reproduced with permission. Copyright 2021, American Chemical Society. (D) The left inset is a schematic showing the structural similarity between neuron-like electronics and neurons, the middle inset is a fluorescence microscope image of a neuron and false-colored SEM images of two neuron-like electronics designs, and the right inset is bending stiffness of axons, neuron-like electronics and examples of previously reported [152]. Reproduced with permission. Copyright 2021, American Chemical Society.

comparable to those obtained by the patch-clamp electrodes (Figure 8B). Different from invasive BCIs, functional calcium imaging is another method to record the neural activity of thousands of neurons without causing damage to the tissues. However, this method faces a critical challenge of low temporal resolution whose delay is about 10–50 ms. Extracellular recording such as electrocorticography is a non-invasive method which has a high temporal resolution but a low spatial resolution. Therefore, Neto et al. [151] combined the two methods mentioned above and proposed a transparent and flexible electrode based on AgNWs. They used AgNWs and indium zinc oxide to develop hybrid films that are stable under physiological conditions (Figure 8C). Apart from the good mechanical properties, the high aspect ratio of nanowires also enabled the electrode an excellent optical property, which demonstrated transparency over the visible light spectrum from 400 to 1200 nm. Besides, the sheet resistance of this hybrid film is 6 Ω/sq which is the lowest data among transparent electrocorticography electrodes reported. Because of the flexible, transparent, and conductive properties, the electrodes can adhere tightly to brain tissue and record the electrocorticography signal and a view of the large-scale activity of distributed populations of neurons simultaneously.

Most conventional neuro probes employ a needle-shaped design for EEG recording and neurostimulation. The structural and mechanical dissimilarities between the neuro probes and the neuron targets will lead to neuro damage, loss, and neuroinflammation. The capability to design nanowire morphology can be employed to address the issues mentioned above. Inspired by biomimicry and neural structures, in 2019, Yang et al. [152] proposed neuron-like electronics whose building blocks mimicked neurons' structural features and mechanical properties (Figure 8D). As the dimension of neuron-like electronics was reduced to the subcellular scale, the stiffness of neuron-like electronics also decreased 5–20 times compared to state-of-the-art reported probes and was comparable to the axon of a neuron. They implanted the neuron-like electronics into live mice by a stereotaxic injection method. After experiments and long-term observation, it demonstrated that the immune response of neuron-like electronics was negligible and could form a seamless interpenetrating interface with the brain after a few days. Specifically, the neuron-like electronics exhibited excellent stability in recording EEG signals, which kept recording individual cells without quality loss for at least 3 months after implantation. Because of the similar structure and mechanical properties, the neuron-like electronics could minimize to a large extent the influence of micromotion and tissue damage and keep a stable recording.

5 | Applications in Artificial Skins

Skin is the largest organ in the human body, protecting us from external environmental factors, regulating homeostasis, including body temperature, and mediating touch, which allows the detection of various internal and external disturbances, such as pressure, strain, vibration, temperature, pain, and chemicals, performing important functions in the human body. Therefore, there is significant interest in using electronic devices to mimic the functions of human skin, known as electronic skin (e-skin) [153, 154]. The most fundamental characteristic of e-skin lies in its stretchability, which poses a significant challenge to traditional rigid sensors. However, flexible sensors can effectively meet this challenge and be integrated into e-skin. Nanowires serve as excellent functional carriers in flexible sensing, offering high sensitivity, good mechanical properties, excellent optical transparency, and customizable morphological features, enabling high-precision and even integrated functionalities such as tactile sensing, energy harvesting and storage, and synchronized heating [155–157]. E-skin not only serves as a system to partially replace the functions of human skin, such as injury warnings, body temperature monitoring and maintenance, and recognition of body movements and sign language, but also focuses on functions beyond those of human skin, such as energy harvesting and storage, and enhancement of VR technology. It is foreseeable that e-skin, as a new generation of sensors, has broad prospects for development and application.

5.1 | Tactile Sensing

Tactile sensing is an important function of human skin. It can not only help people perceive the objects they touch to complete various complex tasks but also alert them when they encounter danger. Tactile sensors can be widely used in clinical treatment and human–machine interfaces. Because of inherent genetic mutations or acquired brain lesions, some people lose the capacity for tactile perception, which will limit normal daily life and put them at risk of danger without their awareness. Besides, during the process of transmitting signals from the human body perception to the machine, and then transmitting signals back from the machine's perception of the external environment, it also owes to the role of tactile sensing. Therefore, significant attention and effort have been devoted to inventing an artificial skin to realize high-performance tactile sensing. In 2018, Li et al. [158] proposed a flexible, stretchable, and sensitive piezoresistive sensor with a structured AgNWs-PDMS composite. They used Ni foam as a sacrificial template of sensors and subsequently uniformly coated AgNWs on the Ni foam by spin coating as the inner surface of tactile sensors. Finally, they infiltrated the PDMS into the AgNWs/Ni foam to construct the structure of this sensor and used hydrochloric acid to remove the Ni foam (Figure 9A). The hollow microstructure enabled the sensor to have a high-sensitivity piezoresistive effect. When the tactile sensor deformed under the external force, the contact area of the inner surface and the distance of AgNWs also changed and led to a change of resistance. Through the theory, the current of the sensor showed a linear relationship with pressure force and could detect a very small force even to mouth blowing. Besides, this tactile sensor performed a low response time of about 90 ms and a stable mechanical property, which operated properly over 2000 cycles of bending/unbending, which could promise real-time tactile sensing. However, the change of electrical signal may not be intuitive and has a low spatial resolution. Therefore, as shown in Figure 9B, Zhang et al. [159] proposed a dual-mode electronic skin, which combined electrical and optical responses. They developed a liquid nitrogen-assisted transfer method to transfer an ultrathin AgNW network onto the elastic PDMS

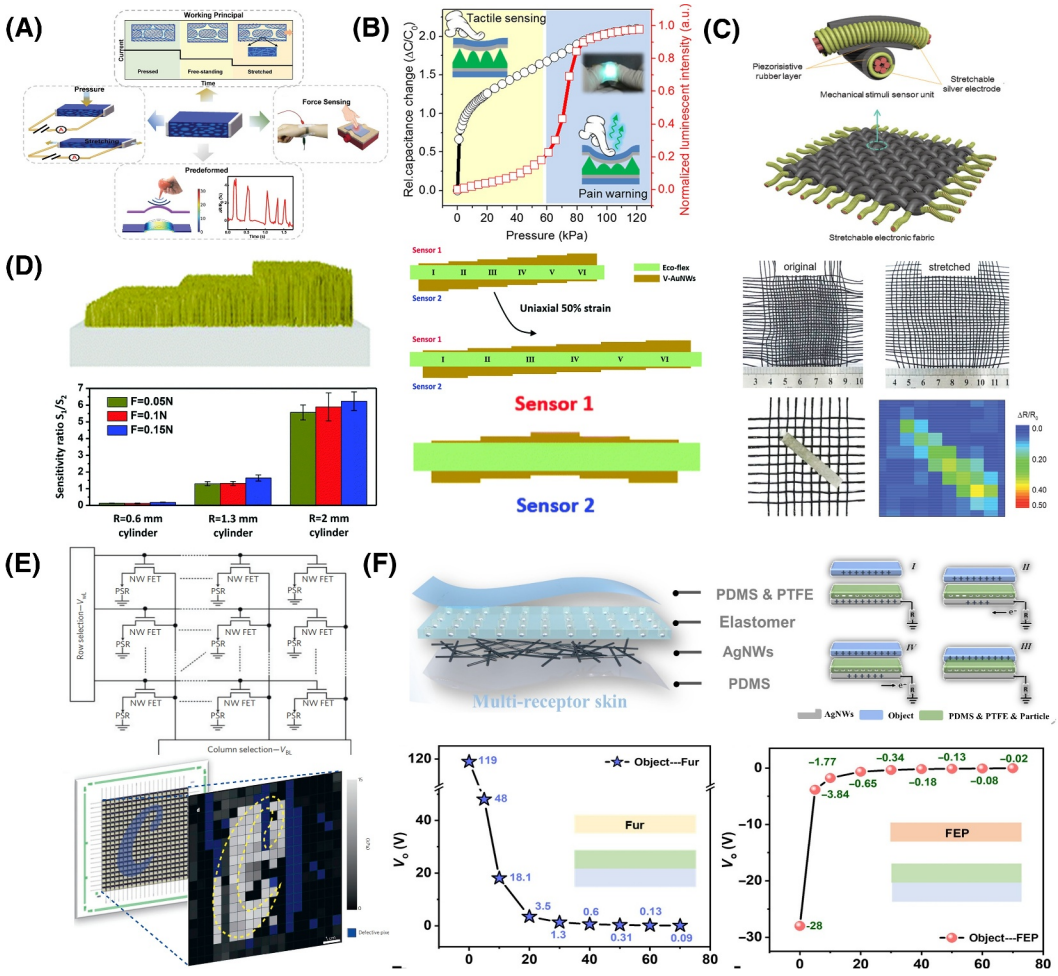

FIGURE 9 | (A) Working schematics of sensor based on AgNWs-PDMS composite and applications [158]. Reproduced with permission. Copyright 2018, WILEY-VCH Verlag GmbH & Co. KGaA, Weinheim. (B) Dual-mode sensing behavior and the inset show the high-magnification optical image of the dashed square [159]. Reproduced with permission. Copyright 2017, American Chemical Society. (C) The top inset is the schematic of electronic fabric with fibrous sensor units and the bottom inset is the optical images of the electronic fabric and corresponding 2D intensity profile of resistance changes [160]. Reproduced with permission. Copyright 2015, WILEY-VCH Verlag GmbH & Co. KGaA, Weinheim. (D) The top inset is the schematic of a location-specific sensor under a uniaxial strain of 50% and the bottom insets are the schematic of staircase concentric sensor structural design and sharpness-specific parameter independent of the forces applied [161]. Reproduced with permission. Copyright 2018, The Royal Society of Chemistry. (E) The top inset is the circuit schematic of the active matrix and the bottom inset is the design layout of the sensor device and the corresponding 2D intensity profile [162]. Reproduced with permission. Copyright 2010, Macmillan Publishers Limited. (F) The top inset is the schematic diagram of the multi-receptor skin and the bionic electroreceptor working mechanism for tele-perception, and the bottom inset is the output voltage of the fur and fluorinated ethylene propylene layer approaching the bionic electroreceptor respectively [163]. Reproduced under terms of the CC-BY license. Copyright 2024, The Authors, published by The American Association for the Advancement of Science.

substrate as the flexible electrodes of the capacitor. Besides, they used an etched silicon wafer as a mold to fabricate the surface microstructure of PDMS, which was mixed with ZnS/Cu phosphor particles serving as the luminescent layer and dielectric layer. When the tactile sensor was subjected to external force, the distance between the top and down electrodes changed and led to a change in capacitance. However, the high sensitivity of the electrical response gradually decreased as the pressure force increased. When the external force was enhanced to a certain level, the decreasing distance led to a high electrical field on the dielectric layer. The ZnS/Cu phosphor particles were triggered and emitted light as a danger alert for significant pressure. This dual-mode sensor provided static and dynamic tactile sensing with a wide measurement range.

To mimic the ability of human skin to sense multiple mechanical stimuli, nanowires can be integrated with fiber to fabricate flexible and conductive electric fibers. As shown in Figure 9C, Ge et al. [160] proposed a stretchable sensor array composed of conductive fibers, which could map and quantify multiple mechanical stresses. They used the elastic thread with inner polyurethane fibers helically wound by nylon fiber as the framework of the coaxial structure. Then they stretched the elastic thread to 100% of tensile strain and used a facile dip-coating process to coat AgNWs onto the surface of the elastic thread to guarantee a thorough encapsulation. Finally, the AgNW elastic thread was coated with stretchable and piezoresistive rubber through a dip-coating process and the composite fibers were obtained. As the composite fibers were stacked perpendicularly, they formed a cross-contact point whose area

influenced the resistance and performed a piezoresistive effect. Therefore, using composite fibers to construct a sensor array enables detection of both the position and exact value of mechanical stimuli by measuring the resistance between each row and vertical contact. Besides, the coaxial structure of composite fibers demonstrated a stable sensitivity and high mechanical stability. Designing pixelated sensor arrays to mimic the ability of human skin to perceive multidimensional signals always needs numerous wiring interconnections. Therefore, Gong et al. [161] proposed a tactile electronic skin sensor that could obviously reduce the number of pixels and achieve a large-area pressure mapping and sharpness-specific tactile. They first grew vertical AuNWs on the flexible Ecoflex substrates by a modified seed-mediated approach and subsequently used a PI mask to passivate selected regions of AuNWs. As the rest region of AuNWs continued to grow, they formed a staircase structure. By this method, they designed a back-to-back linear or spiral assembly of two staircase structures, which could separately achieve pressure mapping and sharpness-specific tactile, as the longer AuNWs exhibited lower pressure sensitivity because of their lower base resistance. Besides, this tactile sensor exhibited a stable mechanical property under a repeated strain for over 2000 cycles with a reversible resistance change and functioned normally in stretched states.

Apart from the above passive devices, integrating NW-FETs with flexible substrates as the active-matrix tactile sensor is also an important solution to fabricate artificial skin. Takei et al. [162] proposed a flexible and low-voltage pressure-sensor array with a macroscale integration of parallel Ge/Si nanowires. They used parallel arrays of nanowires as the channel of FETs, which reduced the random variation of device performance. Simultaneously, they used a laminated pressure-sensitive rubber to connect the source of NW-FETs with the ground and functioned as the sensing element (Figure 9E). As the pressure was applied to the devices, the conductance of the pressure-sensitive rubber would change, which modulates the characteristics of NW-FETs. Each NW-FET worked as a pixel of the tactile sensor. By monitoring the conductance of every pixel, it could realize a high spatial resolution pressure mapping. Besides, the small dimensions of nanowires enabled the tactile sensor to have a high flexibility and mechanical robustness, whose sensing performance did not degrade after over 2000 bending cycles with a curvature radius of 2.5 mm. Besides, different from conventional tactile sensors relying on direct physical contact, Du et al. [163] proposed a novel tele-perception noncontact sensor inspired by the dual sensory system and arrangement of receptors of the platypus. In this tele-perception tactile sensor, they coated a layer of AgNWs on the flexible PDMS substrate as the electrodes and embedded inorganic nonmetal nanoparticles into a layer of elastomer with the help of silicon wafer templates, which facilitated the dielectric polarization and generated triboelectric electricity (Figure 9F). This sensor realized a high sensitivity, signal stability, and tele-perception tactile sensing with a $\Delta V / \Delta d$ sensitivity of 14.2.

5.2 | Novel Structure and Application

The human skin can detect different external signals such as strain, pressure, temperature, and so on, and converts these signals and transmits them back to the brain. Therefore, an electronic skin capable of sensing multiple physical quantities has long been sought after. However, different physical signals may involve different detecting mechanisms and need different structures or materials, which presents a significant challenge for achieving cost-effective multimodal sensors. As shown in Figure 10A, Gong et al. [164] proposed a scalable multifunctional electronic tattoo with a programmable local cracking technology. They first sputtered a metal thin film onto the specific location of the vertically AuNWs by shadow masks and applied repeated tensile stretching to form stable cracks. Finally,

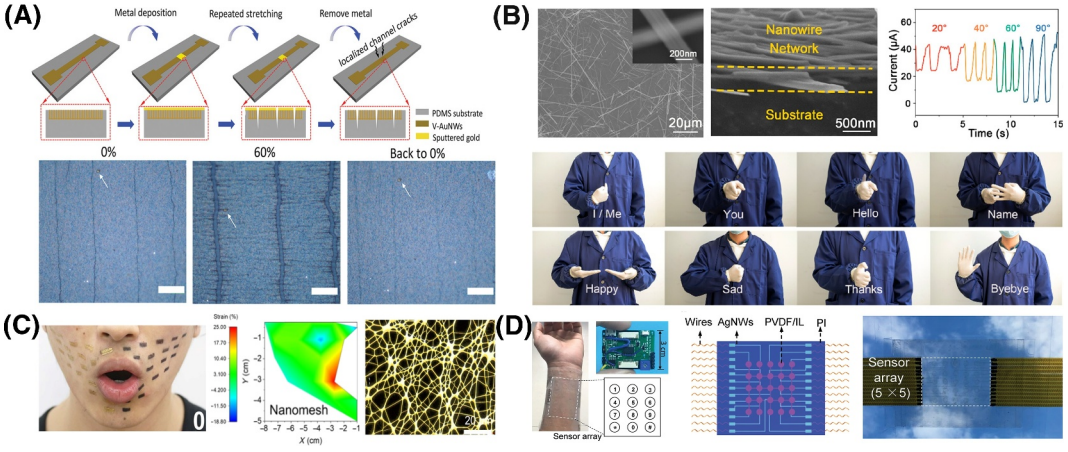

FIGURE 10 | (A) The top inset is the schematic of the fabrication process of localized cracks and the bottom inset is optical images of a cracked film [164]. Reproduced with permission. Copyright 2019, WILEY-VCH Verlag GmbH & Co. KGaA, Weinheim. (B) The top inset is vertical and cross-sectional SEM images of the nanowire network and the current signals from the e-skin and the bottom inset is partially representative of sign language gestures [165]. Reproduced with permission. Copyright 2023, American Chemical Society. (C) The left inset is a photograph of a face during the speech of "o", the middle inset is strain mapping of the right side of the face, and the right inset is the microscopic characterization of PDMS/hexane [166]. (D) The left inset is a photograph of the wearable smart band, the middle inset is a schematic illustration of a smart window, and the right inset is a photo of a smart window [167]. Reproduced under terms of the CC-BY license. Copyright 2020, The Authors, published by WILEY-VCH Verlag GmbH & Co. KGaA, Weinheim.

after removing the metal thin film, parallel channel cracks remained on the sensor. Using this method, they could program the size, shape, and orientation of cracks to realize different functions. The noncracked areas exhibited an average gauge factor of about 0.17 of the strain sensitivity, but the cracked areas performed a notable gauge factor of about 1035 because crack enlargement led to a sharp reduction in conductivity. Based on this principle, they developed strain or pressure sensors, anisotropic orientation-specific sensors, and so on. Besides, they utilized the noncracked serpentine pattern to fabricate temperature sensors whose relative resistance was linear to the change in the temperature. Additionally, this temperature sensor exhibited a good sensitivity that was comparable to those of the commercial products. These sensors with different functions could be easily integrated to achieve multifunctional electronic skin.

Besides, from sensing the external signal, the artificial skin also can be used to monitor the movement of humans, such as gesture signals, facial expressions, and so on. These functions can be widely applied in fields such as healthcare, human–machine interfaces, and others. In 2023, Zhao et al. [165] presented breathable piezoresistive electronic skins based on Mo_2S_3 nanowire networks (Figure 10B). They proposed a synthesizing mechanism to fabricate Mo_2S_3 nanowires by a molten-salt-assisted reaction. This Mo_2S_3 nanowire exhibited a high conductivity of 4.9×10^4 S m^{-1} and a high aspect ratio of about 200. Subsequently, they used a liquid–liquid interface self-assembly method to fabricate an ultrathin Mo_2S_3 nanowire network, which exhibited a high piezoresistive sensitivity, a very low response limit of 0.08 Pa, and a high durability over 3000 cycles. Besides, the high sensitivity, good biocompatibility, and fast response time enabled the artificial skin to realize gesture recognition with a high accuracy by attaching it to each finger joint to form a wearable system. Besides, Wang et al. [166] proposed an ultrathin and durable nano-mesh strain sensor that could be used to monitor the strain mapping of facial skin (Figure 10C). The thickness of artificial skins faced a trade-off between the mechanical property and wearing experience. A large thickness may enable artificial skins to have a good stretchability and durability, but also brought people discomfort. Their team used polyurethane nanowires as the core and PDMS as the sheath to fabricate ultralight nano-meshes with a thickness of about 430 nm. With such a small thickness, the nano-meshes exhibited an excellent mechanical property, which could bear 5000 cycles of stretching/releasing at 60% strain with a very small change of resistance. The artificial skin was attached to the user's face skin during the speech for 3.5 h and was demonstrated to realize a strain mapping with minimum mechanical interference without causing any discomfort to the wearer. Additionally, transparency is also a key requirement for electronic skin. Liu et al. [167] proposed a flexible and transparent capacitive-type pressure sensor. They transferred an ultrathin AgNW film on a thin PI substrate by spray-coating as the electrodes of capacitance (Figure 10D). Because of the high aspect ratio of AgNWs with a diameter of about 30 nm and an average length of about 30 μm, the electrodes exhibited a high transparency of 90.4%. They immersed porous PVDF membrane into the ionic liquid to fabricate a highly transparent dielectric layer for the capacitance. This transparent, flexible, and very thin capacitance pressure sensor could be attached to the surface of the skin as a transparent wearable band and a smart window as shown in Figure 10D and had a wide application in human–machine interfaces.

6 | Conclusions and Perspectives

In this review, we systematically explore the advanced fabrication techniques and developments of nanowire-based flexible sensors in the fields of wearable electronics, BCIs, and artificial skins, which are primarily driven by the increasing demands for health monitoring, industrial innovation, and daily life convenience in the era of smart technologies. As a quasi-1D material, nanowires with high aspect ratios, excellent electrical properties, and superior mechanical performance, are an ideal choice for the development of high-performance flexible electronics. Additionally, the good biocompatibility and minimal tissue damage associated with nanowires are crucial for achieving long-term, stable, and high-performance EEG monitoring and stimulation in BCI applications. Over the past decade, extensive research and reports have focused on top–down approaches for nanowire fabrication. Simultaneously, to address challenges related to precise control over nanowire position, morphology, and uniformity, bottom–up growth methods have also been investigated. These collective efforts have led to the development of a mature theoretical framework for synthesizing, transferring, and assembling nanowires. In particular, through the precise control of growth conditions or the use of specific template-assisted techniques, it is possible to finely tune the morphology, composition, and arrangement of nanowires, thereby meeting the requirements of specific applications. In the future, it is anticipated that nanowire-based flexible sensors will find broader applications. This is expected to open up a scalable, cost-effective, and highly productive manufacturing platform, significantly advancing the development of smart sensing technologies.

However, the further development of nanowire-based flexible sensors will require systematic exploration and comprehensive considerations. Key aspects for future development include:

1. Innovations in materials: Developing flexible organic/polymeric dielectric and conductive materials compatible with nanowires will be a key focus of future research. These materials must exhibit good mechanical stability and environmental robustness to ensure the reliability and long-term stability of the entire system.
2. Energy supply and storage: Efficient energy sources and storage technologies are crucial for supporting flexible sensors in wearable, portable, and implantable devices. For example, miniaturized photovoltaic units and optoelectronic devices based on nanowires can power various sensing and communication applications. Additionally, the development of flexible energy storage devices, such as batteries or supercapacitors, will significantly enhance the operational autonomy and reliability of these systems. We have also provided a simple summary of the advantages and disadvantages of common batteries used in flexible sensors in Table 3.

TABLE 3 | Summary of the commonly used battery types for flexible sensors.

Battery type	Advantages	Disadvantages	References
Lithium-ion batteries	High energy density; long cycle life; low self-discharge rate; no memory effect; high voltage per cell	Expensive; requires a charging circuit; safety concerns	[168, 169]
Sodium-ion batteries	Enhanced safety profiles; cost-effectiveness; environmental friendly; abundant resources	Low energy density; sluggish kinetics; volume deformation; low cycle life; poorer performance at low temperatures	[170, 171]
Zinc-ion batteries	Cost-effectiveness; high safety; environmental friendly; abundant resources; deformability of metal zinc	Severe capacity degradation; sluggish kinetics; low cycle life; immature technology	[172, 173]
Lithium/sodium-air batteries	Ultra-high energy density; low self-discharge rate	Safety concerns; air management complexity; electrode degradation; strictly sealed environment	[174, 175]
Zinc/magnesium-air batteries	High theoretical energy densities; biocompatibility; excellent safety; cost-effectiveness; low self-discharge rate	Air management complexity; electrode degradation; immature technology	[174, 176]
Supercapacitors	Extremely fast charging and discharging rates; very long cycle life; high power density; no memory effect	Lower energy density; higher self-discharge rate; expensive	[177, 178]

3. Biocompatibility: Improving the biocompatibility of nanowire materials and optimizing their interfaces with biological tissues are important future directions. To achieve high-precision real-time monitoring and control of neural signals, geometrically optimized probes, FET sensors, or stimulators are required. Integrating on-site signal processing logic and machine learning algorithms will enable more intelligent and precise extraction and processing of bioelectric signals.
4. Multifunctional integration and intelligence: Future flexible nanowire sensors will integrate multiple functions, such as sensing, computing, and communication, into a single complex system. This requires precise design and integration at the nanoscale to achieve highly compact and multifunctional electronic systems. Advanced signal processing algorithms and artificial intelligence will enhance the intelligence of these sensors. For example, adaptive algorithms and machine learning will allow sensors to automatically adjust their operating states to adapt to different environments and application requirements.
5. Manufacturing processes and scalable production: Developing low-cost, high-throughput fabrication methods is essential for large-scale production. Catalytic growth techniques, particularly low-temperature, high-throughput processes, offer a promising alternative to traditional lithography, enabling the scalable production of well-ordered nanowire arrays.

Regarding the industrial production of nanowire-based flexible sensors, those flexible sensors with relaxed precision requirements are already integrated into manufacturing processes, whereas those needing precise nanowire placement still encounter challenges that hinder large-scale production. Although c-Si technology and its adaptation for flexibility show significant potential, several challenges impede its commercialization for large-scale production. First, developing reliable processes for growing or transferring flexible c-Si requires overcoming technical challenges in materials science while ensuring high compatibility with existing semiconductor manufacturing equipment and process flows. Second, as manufacturing processes mature and technological innovations advance, alongside the continuous expansion of the silicon-based materials market, it is crucial to continuously innovate in production processes to improve manufacturing techniques and reduce costs when scaling up silicon material production. Cost reduction is critical; catalytic growth has shown advantages, but issues such as uniformity must be addressed. Although successful control of size and orientation of catalytically grown SiNWs has been achieved using VLS and IPSLS methods, high-precision deterministic growth control remains challenging regarding diameter uniformity and repeatability. This necessitates ongoing innovation in growth or post-growth adjustment technologies to meet the high standards set by mainstream "top–down" c-Si technologies.

To address these challenges and promote future development, several strategies can be pursued:

1. Process integration: Develop integrated manufacturing processes that streamline workflows by combining multiple steps, reducing complexity, and enhancing efficiency. For instance, optimizing VLS and IPSLS methods can lead to better control over the size and orientation of SiNWs, improving uniformity and consistency.
2. Material innovation: Explore novel materials and catalysts that increase growth rates and minimize defects, thereby boosting yields. Innovations in materials can also open up new application areas, further expanding the market.
3. Automation and scaling: Implement automation technologies and scalable production lines to increase throughput and lower costs. Automation not only enhances precision

but also ensures product quality consistency, which is vital for mass production.

4. Standardization: Establish industry standards for nanowire fabrication to ensure consistency and interoperability across different applications. Standardization can lower barriers to entry and foster cross-industry collaboration and exchange, driving industry-wide progress.

In summary, the future development of nanowire-based flexible sensors requires a systematic approach that considers materials, integration technologies, energy supply, biocompatibility, multifunctional integration, and manufacturing processes. Through interdisciplinary collaboration and technological innovation, nanowire-based flexible sensors have the potential to play a significant role in healthcare, human–machine interaction, and other high-tech fields, bringing about transformative changes.

Acknowledgments

The authors acknowledge the financial support received from the National Key Research Program of China (No. 92164201), National Natural Science Foundation of China for Distinguished Young Scholars (No. 62325403), Natural Science Foundation of Jiangsu Province (BK20230498), Jiangsu Funding Program for Excellent Postdoctoral Talent (2024ZB427), and the National Natural Science Foundation of China (61934004).

Conflicts of Interest

The authors declare no conflicts of interest.

Data Availability Statement

No primary research results, software or codes have been included and no new data were generated or analyzed as part of this review.

References

1. A. Nag, S. C. Mukhopadhyay, and J. Kosel, "Wearable Flexible Sensors: A Review," *IEEE Sensors Journal* 17, no. 13 (2017): 3949–3960, https://doi.org/10.1109/jsen.2017.2705700.

2. Y. Luo, M. R. Abidian, J. H. Ahn, et al., "Technology Roadmap for Flexible Sensors," *ACS Nano* 17, no. 6 (2023): 5211–5295, https://doi.org/10.1021/acsnano.2c12606.

3. N. Wen, L. Zhang, D. Jiang, et al., "Emerging Flexible Sensors Based on Nanomaterials: Recent Status and Applications," *Journal of Materials Chemistry A* 8, no. 48 (2020): 25499–25527, https://doi.org/10.1039/D0TA09556G.

4. Z. Ren, J. Yang, D. Qi, et al., "Flexible Sensors Based on Organic–Inorganic Hybrid Materials," *Advanced Materials Technologies* 6, no. 4 (2021): 2000889, https://doi.org/10.1002/admt.202000889.

5. E. Liu, Z. Cai, Y. Ye, M. Zhou, H. Liao, and Y. Yi, "An Overview of Flexible Sensors: Development, Application, and Challenges," *Sensors* 23, no. 2 (2023): 817, https://doi.org/10.3390/s23020817.

6. G. Shen, "Recent Advances of Flexible Sensors for Biomedical Applications," *Progress in Natural Science: Materials International* 31, no. 6 (2021): 872–882, https://doi.org/10.1016/j.pnsc.2021.10.005.

7. C. Pang, C. Lee, and K. Y. Suh, "Recent Advances in Flexible Sensors for Wearable and Implantable Devices," *Journal of Applied Polymer Science* 130, no. 3 (2013): 1429–1441, https://doi.org/10.1002/app.39461.

8. H. Liu, L. Wang, G. Lin, and Y. Feng, "Recent Progress in the Fabrication of Flexible Materials for Wearable Sensors," *Biomaterials Science* 10, no. 3 (2022): 614–632, https://doi.org/10.1039/d1bm01136g.

9. Z. Cui, W. Wang, L. Guo, et al., "Haptically Quantifying Young's Modulus of Soft Materials Using a Self-Locked Stretchable Strain Sensor," *Advances in Materials* 34, no. 25 (2022): e2104078, https://doi.org/10.1002/adma.202104078.

10. Y. Sun, H. Tai, Z. Yuan, Z. Duan, Q. Huang, and Y. Jiang, "A Facile Strategy for Low Young's Modulus PDMS Microbeads Enhanced Flexible Capacitive Pressure Sensors," *Particle & Particle Systems Characterization* 38, no. 7 (2021): 2100019, https://doi.org/10.1002/ppsc.202100019.

11. R. Chen, X. Xu, D. Yu, et al., "Highly Stretchable and Fatigue Resistant Hydrogels With Low Young's Modulus as Transparent and Flexible Strain Sensors," *Journal of Materials Chemistry C* 6, no. 41 (2018): 11193–11201, https://doi.org/10.1039/c8tc02583e.

12. S. T. Han, H. Peng, Q. Sun, et al., "An Overview of the Development of Flexible Sensors," *Advances in Materials* 29, no. 33 (2017): 1700375, https://doi.org/10.1002/adma.201700375.

13. G. Huang and Y. Mei, "Thinning and Shaping Solid Films Into Functional and Integrative Nanomembranes," *Advances in Materials* 24, no. 19 (2012): 2517–2546, https://doi.org/10.1002/adma.201200574.

14. K. He, Y. Jiang, T. Wang, et al., "Assemblies and Composites of Gold Nanostructures for Functional Devices," *Aggregate* 3, no. 4 (2021): e57, https://doi.org/10.1002/agt2.57.

15. J. C. Costa, F. Spina, P. Lugoda, L. Garcia-Garcia, D. Roggen, and N. Münzenrieder, "Flexible Sensors—From Materials to Applications," *Technologies* 7, no. 2 (2019): 35, https://doi.org/10.3390/technologies7020035.

16. M. Amjadi, K. U. Kyung, I. Park, and M. Sitti, "Stretchable, Skin-Mountable, and Wearable Strain Sensors and Their Potential Applications: A Review," *Advanced Functional Materials* 26, no. 11 (2016): 1678–1698, https://doi.org/10.1002/adfm.201504755.

17. C. Yan, J. Wang, W. Kang, et al., "Highly Stretchable Piezoresistive Graphene-Nanocellulose Nanopaper for Strain Sensors," *Advances in Materials* 26, no. 13 (2014): 2022–2027, https://doi.org/10.1002/adma.201304742.

18. Y. Yao, W. Huang, J. Chen, et al., "Flexible and Stretchable Organic Electrochemical Transistors for Physiological Sensing Devices," *Advances in Materials* 35, no. 35 (2023): e2209906, https://doi.org/10.1002/adma.202209906.

19. X. Xu, Y. Zhao, and Y. Liu, "Wearable Electronics Based on Stretchable Organic Semiconductors," *Small* 19, no. 20 (2023): e2206309, https://doi.org/10.1002/smll.202206309.

20. H. Ling, S. Liu, Z. Zheng, and F. Yan, "Organic Flexible Electronics," *Small Methods* 2, no. 10 (2018): 1800070, https://doi.org/10.1002/smtd.201800070.

21. C. Zhang, H. Dong, C. Zhang, Y. Fan, J. Yao, and Y. S. Zhao, "Photonic Skins Based on Flexible Organic Microlaser Arrays," *Science Advances* 7, no. 31 (2021): eabh3530, https://doi.org/10.1126/sciadv.abh3530.

22. D. J. Lipomi, "Stretchable Figures of Merit in Deformable Electronics," *Advances in Materials* 28, no. 22 (2016): 4180–4183, https://doi.org/10.1002/adma.201504196.

23. B. Hu, W. Chen, and J. Zhou, "High Performance Flexible Sensor Based on Inorganic Nanomaterials," *Sensors and Actuators B: Chemical* 176 (2013): 522–533, https://doi.org/10.1016/j.snb.2012.09.036.

24. T. Wang, Y. Guo, P. Wan, H. Zhang, X. Chen, and X. Sun, "Flexible Transparent Electronic Gas Sensors," *Small* 12, no. 28 (2016): 3748–3756, https://doi.org/10.1002/smll.201601049.

25. E. K. Lee, M. Y. Lee, C. H. Park, H. R. Lee, and J. H. Oh, "Toward Environmentally Robust Organic Electronics: Approaches and

Applications," *Advances in Materials* 29, no. 44 (2017): 1703638, https://doi.org/10.1002/adma.201703638.

26. Z. Shen, W. Huang, L. Li, et al., "Research Progress of Organic Field-Effect Transistor Based Chemical Sensors," *Small* 19, no. 41 (2023): e2302406, https://doi.org/10.1002/smll.202302406.

27. S. Liu, X. Xu, and J. Jiang, "Flexible Transparent ITO Thin Film With High Conductivity and High-Temperature Resistance," *Ceramics International* 50, no. 22 (2024): 47649–47654, https://doi.org/10.1016/j.ceramint.2024.09.110.

28. P. K. Hiroli, S. Varun, S. Mudhulu, B. Kathik, S. Mahendra Kumar, and C. Manjunatha, "ITO Conductive Ink: Advances in Materials, Preparation, and Potential Sensor Applications," *ECS Transactions* 107, no. 1 (2022): 20135–20146, https://doi.org/10.1149/10701.20135ecst.

29. Q. Hu, S. Zhu, C. Gu, S. Liu, M. Zeng, and Y. Wu, "Ultrashort 15-nm Flexible Radio Frequency ITO Transistors Enduring Mechanical and Temperature Stress," *Science Advances* 8, no. 51 (2022): eade4075, https://doi.org/10.1126/sciadv.ade4075.

30. X. Zhang, Y. Chen, W. Zhang, et al., "Synergetic Design of Transparent Topcoats on ITO-Coated Plastic Substrate to Boost Surface Erosion Performance," *Coatings* 11, no. 12 (2021): 1448, https://doi.org/10.3390/coatings11121448.

31. Y. G. Bi, Y. F. Liu, X. L. Zhang, et al., "Ultrathin Metal Films as the Transparent Electrode in ITO-Free Organic Optoelectronic Devices," *Advanced Optical Materials* 7, no. 6 (2019): 1800778, https://doi.org/10.1002/adom.201800778.

32. T. Sekitani and T. Someya, "Stretchable, Large-Area Organic Electronics," *Advances in Materials* 22, no. 20 (2010): 2228–2246, https://doi.org/10.1002/adma.200904054.

33. A. Iqbal, J. Hong, T. Y. Ko, and C. M. Koo, "Improving Oxidation Stability of 2D MXenes: Synthesis, Storage Media, and Conditions," *Nano Convergence* 8, no. 1 (2021): 9, https://doi.org/10.1186/s40580-021-00259-6.

34. X. Zhan, C. Si, J. Zhou, and Z. Sun, "MXene and MXene-Based Composites: Synthesis, Properties and Environment-Related Applications," *Nanoscale Horizons* 5, no. 2 (2020): 235–258, https://doi.org/10.1039/c9nh00571d.

35. C. Zhang and V. Nicolosi, "Graphene and MXene-Based Transparent Conductive Electrodes and Supercapacitors," *Energy Storage Materials* 16 (2019): 102–125, https://doi.org/10.1016/j.ensm.2018.05.003.

36. E. B. Aydın and M. K. Sezgintürk, "Indium Tin Oxide (ITO): A Promising Material in Biosensing Technology," *TrAC, Trends in Analytical Chemistry* 97 (2017): 309–315, https://doi.org/10.1016/j.trac.2017.09.021.

37. T. Cheng, Y. Zhang, W. Y. Lai, and W. Huang, "Stretchable Thin-Film Electrodes for Flexible Electronics With High Deformability and Stretchability," *Advances in Materials* 27, no. 22 (2015): 3349–3376, https://doi.org/10.1002/adma.201405864.

38. J. Zhang, T. Sun, Y. Chen, et al., "Nanowires in Flexible Sensors: Structure Is Becoming a Key in Controlling the Sensing Performance," *Advanced Materials Technologies* 7, no. 12 (2022): 2200163, https://doi.org/10.1002/admt.202200163.

39. Z. Liu, J. Xu, D. Chen, and G. Shen, "Flexible Electronics Based on Inorganic Nanowires," *Chemical Society Reviews* 44, no. 1 (2015): 161–192, https://doi.org/10.1039/c4cs00116h.

40. N. S. Ramgir, Y. Yang, and M. Zacharias, "Nanowire-Based Sensors," *Small* 6, no. 16 (2010): 1705–1722, https://doi.org/10.1002/smll.201000972.

41. M. J. Zheng, L. D. Zhang, G. H. Li, and W. Shen, "Fabrication and Optical Properties of Large-Scale Uniform Zinc Oxide Nanowire Arrays by One-Step Electrochemical Deposition Technique," *Chemical Physics Letters* 363, no. 1–2 (2002): 123–128, https://doi.org/10.1016/s0009-2614(02)01106-5.

42. M. A. Lim, D. H. Kim, C. O. Park, et al., "A New Route toward Ultrasensitive, Flexible Chemical Sensors: Metal Nanotubes by Wet-Chemical Synthesis along Sacrificial Nanowire Templates," *ACS Nano* 6, no. 1 (2012): 598–608, https://doi.org/10.1021/nn204009m.

43. T. Araki, J. Jiu, M. Nogi, et al., "Low Haze Transparent Electrodes and Highly Conducting Air Dried Films With Ultra-Long Silver Nanowires Synthesized by One-Step Polyol Method," *Nano Research* 7, no. 2 (2013): 236–245, https://doi.org/10.1007/s12274-013-0391-x.

44. Y. Lee, J. Kim, H. Joo, M. S. Raj, R. Ghaffari, and D. Kim, "Wearable Sensing Systems With Mechanically Soft Assemblies of Nanoscale Materials," *Advanced Materials Technologies* 2, no. 9 (2017): 1700053, https://doi.org/10.1002/admt.201700053.

45. J. Shi, L. Wang, Z. Dai, et al., "Multiscale Hierarchical Design of a Flexible Piezoresistive Pressure Sensor With High Sensitivity and Wide Linearity Range," *Small* 14, no. 27 (2018): e1800819, https://doi.org/10.1002/smll.201800819.

46. D. Son, J. Kang, O. Vardoulis, et al., "An Integrated Self-Healable Electronic Skin System Fabricated via Dynamic Reconstruction of a Nanostructured Conducting Network," *Nature Nanotechnology* 13, no. 11 (2018): 1057–1065, https://doi.org/10.1038/s41565-018-0244-6.

47. B. Patella, R. R. Russo, A. O'Riordan, G. Aiello, C. Sunseri, and R. Inguanta, "Copper Nanowire Array as Highly Selective Electrochemical Sensor of Nitrate Ions in Water," *Talanta* 221 (2021): 121643, https://doi.org/10.1016/j.talanta.2020.121643.

48. Y. P. Palve and N. Jha, "A Novel Bilayer of Copper Nanowire and Carbon Nanotube Electrode for Highly Sensitive Enzyme Free Glucose Detection," *Materials Chemistry and Physics* 240 (2020): 122086, https://doi.org/10.1016/j.matchemphys.2019.122086.

49. H. Lee, M. Kim, I. Kim, et al., "Flexible and Stretchable Optoelectronic Devices Using Silver Nanowires and Graphene," *Advances in Materials* 28, no. 22 (2016): 4541–4548, https://doi.org/10.1002/adma.201505559.

50. Y. Ding, S. Xiong, L. Sun, et al., "Metal Nanowire-Based Transparent Electrode for Flexible and Stretchable Optoelectronic Devices," *Chemical Society Reviews* 53, no. 15 (2024): 7784–7827, https://doi.org/10.1039/d4cs00080c.

51. Z. Yang, L. Guo, B. Zu, Y. Guo, T. Xu, and X. Dou, "CdS/ZnO Core/Shell Nanowire-Built Films for Enhanced Photodetecting and Optoelectronic Gas-Sensing Applications," *Advanced Optical Materials* 2, no. 8 (2014): 738–745, https://doi.org/10.1002/adom.201400086.

52. Z. Wu, Y. Xing, W. Ren, Y. Wang, and H. Guo, "Ballistic Transport in Bent-Shaped Carbon Nanotubes," *Carbon* 149 (2019): 364–369, https://doi.org/10.1016/j.carbon.2019.04.062.

53. Y. Wei, S. Chen, F. Li, Y. Lin, Y. Zhang, and L. Liu, "Highly Stable and Sensitive Paper-Based Bending Sensor Using Silver Nanowires/Layered Double Hydroxides Hybrids," *ACS Applied Materials and Interfaces* 7, no. 26 (2015): 14182–14191, https://doi.org/10.1021/acsami.5b03824.

54. C. C. Wu, "Silicon Nanowires Length and Numbers Dependence on Sensitivity of the Field-Effect Transistor Sensor for Hepatitis B Virus Surface Antigen Detection," *Biosensors* 12, no. 2 (2022): 115, https://doi.org/10.3390/bios12020115.

55. H. Kan, M. Li, J. Luo, et al., "PbS Nanowires-on-Paper Sensors for Room-Temperature Gas Detection," *IEEE Sensors Journal* 19, no. 3 (2019): 846–851, https://doi.org/10.1109/jsen.2018.2879895.

56. X. Song, R. Hu, S. Xu, et al., "Highly Sensitive Ammonia Gas Detection at Room Temperature by Integratable Silicon Nanowire Field-Effect Sensors," *ACS Applied Materials and Interfaces* 13, no. 12 (2021): 14377–14384, https://doi.org/10.1021/acsami.1c00585.

57. X. Song, T. Zhang, L. Wu, et al., "Highly Stretchable High-Performance Silicon Nanowire Field Effect Transistors Integrated on Elastomer Substrates," *Advanced Science* 9, no. 9 (2022): e2105623, https://doi.org/10.1002/advs.202105623.

58. X. Song, L. Wu, Y. Liang, et al., "High-Performance Transparent Silicon Nanowire Thin Film Transistors Integrated on Glass Substrates via a Room Temperature Solution Passivation," *Advanced Electronic Materials* 9, no. 4 (2023): 2201236, https://doi.org/10.1002/aelm.202201236.

59. R. G. Hobbs, N. Petkov, and J. D. Holmes, "Semiconductor Nanowire Fabrication by Bottom-Up and Top-Down Paradigms," *Chemistry of Materials* 24, no. 11 (2012): 1975–1991, https://doi.org/10.1021/cm300570n.

60. O. Sahin, O. M. Albayrak, and M. K. Yapici, "Optimization of E-Beam Lithography Parameters for Nanofabrication of Sub-50 nm Gold Nanowires and Nanogaps Based on a Bilayer Lift-Off Process," *Nanotechnology* 35, no. 39 (2024): 395301, https://doi.org/10.1088/1361-6528/ad5e89.

61. M. C. Sun, G. Kim, J. H. Lee, et al., "Patterning of Si Nanowire Array With Electron Beam Lithography for Sub-22 nm Si Nanoelectronics Technology," *Microelectronic Engineering* 110 (2013): 141–146, https://doi.org/10.1016/j.mee.2013.03.023.

62. J. Huang, D. Fan, Y. Ekinci, and C. Padeste, "Fabrication of Ultra-high Resolution Metal Nanowires and Nanodots through EUV Interference Lithography," *Microelectronic Engineering* 141 (2015): 32–36, https://doi.org/10.1016/j.mee.2015.01.016.

63. E. Koren, J. K. Hyun, U. Givan, E. R. Hemesath, L. J. Lauhon, and Y. Rosenwaks, "Obtaining Uniform Dopant Distributions in VLS-Grown Si Nanowires," *Nano Letters* 11, no. 1 (2011): 183–187, https://doi.org/10.1021/nl103363c.

64. A. Mirzaei, M. H. Lee, K. K. Pawar, et al., "Metal Oxide Nanowires Grown by a Vapor-Liquid-Solid Growth Mechanism for Resistive Gas-Sensing Applications: An Overview," *Materials* 16, no. 18 (2023): 6233, https://doi.org/10.3390/ma16186233.

65. T. F. Weng, M. S. Ho, C. Sivakumar, B. Balraj, and P. F. Chung, "VLS Growth of Pure and Au Decorated β-Ga_2O_3 Nanowires for Room Temperature CO Gas Sensor and Resistive Memory Applications," *Applied Surface Science* 533 (2020): 147476, https://doi.org/10.1016/j.apsusc.2020.147476.

66. P. T. Hung, P. D. Hoat, V. X. Hien, et al., "Growth and NO_2-Sensing Properties of Biaxial P-SnO/n-ZnO Heterostructured Nanowires," *ACS Applied Materials and Interfaces* 12, no. 30 (2020): 34274–34282, https://doi.org/10.1021/acsami.0c04974.

67. Y. Liang, W. Qian, R. Hu, et al., "High-Fidelity Moulding Growth and Cross-Section Shaping of Ultrathin Monocrystalline Silicon Nanowires," *Applied Surface Science* 635 (2023): 157635, https://doi.org/10.1016/j.apsusc.2023.157635.

68. L. Yu, M. Oudwan, O. Moustapha, F. Fortuna, and P. Roca i Cabarrocas, "Guided Growth of In-Plane Silicon Nanowires," *Applied Physics Letters* 95, no. 11 (2009), https://doi.org/10.1063/1.3227667.

69. L. Yu, P. J. Alet, G. Picardi, and P. Roca i Cabarrocas, "An In-Plane Solid-Liquid-Solid Growth Mode for Self-Avoiding Lateral Silicon Nanowires," *Physical Review Letters* 102, no. 12 (2009): 125501, https://doi.org/10.1103/PhysRevLett.102.125501.

70. L. Yu, W. Chen, B. O'Donnell, et al., "Growth-in-Place Deployment of In-Plane Silicon Nanowires," *Applied Physics Letters* 99, no. 20 (2011), https://doi.org/10.1063/1.3659895.

71. L. Yu and P. R. i Cabarrocas, "Growth Mechanism and Dynamics of In-Plane Solid-Liquid-Solid Silicon Nanowires," *Physical Review B* 81, no. 8 (2010): 085323, https://doi.org/10.1103/PhysRevB.81.085323.

72. W. Y. Fung, L. Chen, and W. Lu, "Esaki Tunnel Diodes Based on Vertical Si-Ge Nanowire Heterojunctions," *Applied Physics Letters* 99, no. 9 (2011), https://doi.org/10.1063/1.3633347.

73. M. Xu, Z. Xue, L. Yu, et al., "Operating Principles of In-Plane Silicon Nanowires at Simple Step-Edges," *Nanoscale* 7, no. 12 (2015): 5197–5202, https://doi.org/10.1039/c4nr06531j.

74. Z. Xue, M. Sun, T. Dong, et al., "Deterministic Line-Shape Programming of Silicon Nanowires for Extremely Stretchable Springs and Electronics," *Nano Letters* 17, no. 12 (2017): 7638–7646, https://doi.org/10.1021/acs.nanolett.7b03658.

75. M. Xu, J. Wang, Z. Xue, et al., "High Performance Transparent In-Plane Silicon Nanowire Fin-TFTs via a Robust Nano-Droplet-Scanning Crystallization Dynamics," *Nanoscale* 9, no. 29 (2017): 10350–10357, https://doi.org/10.1039/c7nr02825c.

76. Z. Xue, M. Xu, Y. Zhao, et al., "Engineering Island-Chain Silicon Nanowires via a Droplet Mediated Plateau-Rayleigh Transformation," *Nature Communications* 7, no. 1 (2016): 12836, https://doi.org/10.1038/ncomms12836.

77. Z. Xue, M. Xu, X. Li, et al., "In-Plane Self-Turning and Twin Dynamics Renders Large Stretchability to Mono-Like Zigzag Silicon Nanowire Springs," *Advanced Functional Materials* 26, no. 29 (2016): 5352–5359, https://doi.org/10.1002/adfm.201600780.

78. Z. Xue, T. Dong, Z. Zhu, Y. Zhao, Y. Sun, and L. Yu, "Engineering In-Plane Silicon Nanowire Springs for Highly Stretchable Electronics," *Journal of Semiconductors* 39, no. 1 (2018): 011001, https://doi.org/10.1088/1674-4926/39/1/011001.

79. T. Dong, Y. Sun, Z. Zhu, et al., "Monolithic Integration of Silicon Nanowire Networks as a Soft Wafer for Highly Stretchable and Transparent Electronics," *Nano Letters* 19, no. 9 (2019): 6235–6243, https://doi.org/10.1021/acs.nanolett.9b02291.

80. C. Liu, B. Yao, T. Dong, et al., "Highly Stretchable Graphene Nanoribbon Springs by Programmable Nanowire Lithography," *npj 2D Materials and Applications* 3, no. 1 (2019): 23, https://doi.org/10.1038/s41699-019-0105-7.

81. J. Yan, Y. Zhang, Z. Liu, J. Wang, J. Xu, and L. Yu, "Ultracompact Single-Nanowire-Morphed Grippers Driven by Vectorial Lorentz Forces for Dexterous Robotic Manipulations," *Nature Communications* 14, no. 1 (2023): 3786, https://doi.org/10.1038/s41467-023-39524-z.

82. Z. Liu, J. Yan, H. Ma, et al., "Ab Initio Design, Shaping, and Assembly of Free-Standing Silicon Nanoprobes," *Nano Letters* 21, no. 7 (2021): 2773–2779, https://doi.org/10.1021/acs.nanolett.0c04804.

83. S. Zhou and L. Jiang, "Modern Description of Rayleigh's Criterion," *Physical Review A* 99, no. 1 (2019): 013808, https://doi.org/10.1103/PhysRevA.99.013808.

84. L. Li, X. Liu, S. Pal, S. Wang, C. K. Ober, and E. P. Giannelis, "Extreme Ultraviolet Resist Materials for Sub-7 Nm Patterning," *Chemical Society Reviews* 46, no. 16 (2017): 4855–4866, https://doi.org/10.1039/c7cs00080d.

85. M. A. Morris, "Directed Self-Assembly of Block Copolymers for Nanocircuitry Fabrication," *Microelectronic Engineering* 132 (2015): 207–217, https://doi.org/10.1016/j.mee.2014.08.009.

86. P. De Bisschop, "Optical Proximity Correction: A Cross Road of Data Flows," supplement, *Japanese Journal of Applied Physics* 55, no. 6S1 (2016): 06GA01, https://doi.org/10.7567/jjap.55.06ga01.

87. A. Erdmann, H. Mesilhy, and P. Evanschitzky, "Attenuated Phase Shift Masks: A Wild Card Resolution Enhancement for Extreme Ultraviolet Lithography?," *Journal of Micro/Nanopatterning, Materials, and Metrology* 21, no. 2 (2022): 020901, https://doi.org/10.1117/1.Jmm.21.2.020901.

88. F. Zhang, J. Zhu, W. Yue, et al., "An Approach to Increase Efficiency of DOE Based Pupil Shaping Technique for Off-Axis Illumination in Optical Lithography," *Optics Express* 23, no. 4 (2015): 4482–4493, https://doi.org/10.1364/OE.23.004482.

89. J. H. Moon, S. M. Yang, D. J. Pine, and W. S. Chang, "Multiple-Exposure Holographic Lithography With Phase Shift," *Applied Physics Letters* 85, no. 18 (2004): 4184–4186, https://doi.org/10.1063/1.1813644.

90. S. Owa and H. Nagasaka, "Immersion Lithography: Its Potential Performance and Issues," *Optical Microlithography XVI* 5040 (2003): 724–733, https://doi.org/10.1117/12.504599.

91. C. Pan, Z. Luo, C. Xu, et al., "Wafer-Scale High-Throughput Ordered Arrays of Si and Coaxial $Si/Si_{1-x}Ge_x$ Wires: Fabrication, Characterization, and Photovoltaic Application," *ACS Nano* 5, no. 8 (2011): 6629–6636, https://doi.org/10.1021/nn202075z.

92. P. Hashemi, L. Gomez, and J. L. Hoyt, "Gate-All-Around N-MOSFETs With Uniaxial Tensile Strain-Induced Performance Enhancement Scalable to Sub-10-nm Nanowire Diameter," *IEEE Electron Device Letters* 30, no. 4 (2009): 401–403, https://doi.org/10.1109/led.2009.2013877.

93. H. Küpers, A. Tahraoui, R. B. Lewis, et al., "Surface Preparation and Patterning by Nano Imprint Lithography for the Selective Area Growth of GaAs Nanowires on Si(111)," *Semiconductor Science and Technology* 32, no. 11 (2017): 115003, https://doi.org/10.1088/1361-6641/aa8c15.

94. D. Tan, C. Jiang, Q. Li, S. Bi, and J. Song, "Silver Nanowire Networks With Preparations and Applications: A Review," *Journal of Materials Science: Materials in Electronics* 31, no. 18 (2020): 15669–15696, https://doi.org/10.1007/s10854-020-04131-x.

95. C. F. Guo, T. Sun, Q. Liu, Z. Suo, and Z. Ren, "Highly Stretchable and Transparent Nanomesh Electrodes Made by Grain Boundary Lithography," *Nature Communications* 5, no. 1 (2014): 3121, https://doi.org/10.1038/ncomms4121.

96. P. Forrer, F. Schlottig, H. Siegenthaler, and M. Textor, "Electrochemical Preparation and Surface Properties of Gold Nanowire Arrays Formed by the Template Technique," *Journal of Applied Electrochemistry* 30, no. 5 (2000): 533–541, https://doi.org/10.1023/a:1003941129560.

97. Y. Vladimirsky, A. Bourdillon, O. Vladimirsky, W. Jiang, and Q. Leonard, "Demagnification in Proximity X-ray Lithography and Extensibility to 25 nm by Optimizing Fresnel Diffraction," *Journal of Physics D: Applied Physics* 32, no. 22 (1999): L114–L118, https://doi.org/10.1088/0022-3727/32/22/102.

98. C. F. Guo and Z. Ren, "Flexible Transparent Conductors Based on Metal Nanowire Networks," *Materials Today* 18, no. 3 (2015): 143–154, https://doi.org/10.1016/j.mattod.2014.08.018.

99. C. Zhang, X. Miao, K. D. Chabak, and X. Li, "A Review of III–V Planar Nanowire Arrays: Selective Lateral VLS Epitaxy and 3D Transistors," *Journal of Physics D: Applied Physics* 50, no. 39 (2017): 393001, https://doi.org/10.1088/1361-6463/aa7e42.

100. Y. Shan and S. J. Fonash, "Self-Assembling Silicon Nanowires for Device Applications Using the Nanochannel-Guided 'Grow-In-Place' Approach," *ACS Nano* 2, no. 3 (2008): 429–434, https://doi.org/10.1021/nn700232q.

101. Y. Sun, B. Mayers, T. Herricks, and Y. Xia, "Polyol Synthesis of Uniform Silver Nanowires: A Plausible Growth Mechanism and the Supporting Evidence," *Nano Letters* 3, no. 7 (2003): 955–960, https://doi.org/10.1021/nl034312m.

102. Y. X. Zhang, G. H. Li, Y. X. Jin, J. Zhang, and L. Zhang, "Hydrothermal Synthesis and Photoluminescence of TiO_2 Nanowires," *Chemical Physics Letters* 365, no. 3–4 (2002): 300–304, https://doi.org/10.1016/s0009-2614(02)01499-9.

103. C. Zhang, W. Choi, P. K. Mohseni, and X. Li, "InAs Planar Nanowire Gate-All-Around MOSFETs on GaAs Substrates by Selective Lateral Epitaxy," *IEEE Electron Device Letters* 36, no. 7 (2015): 663–665, https://doi.org/10.1109/led.2015.2429680.

104. Y. Sun, T. Dong, L. Yu, J. Xu, and K. Chen, "Planar Growth, Integration, and Applications of Semiconducting Nanowires," *Advances in Materials* 32, no. 27 (2020): e1903945, https://doi.org/10.1002/adma.201903945.

105. T. Sannicolo, M. Lagrange, A. Cabos, C. Celle, J. Simonato, and D. Bellet, "Metallic Nanowire-Based Transparent Electrodes for Next Generation Flexible Devices: A Review," *Small* 12, no. 44 (2016): 6052–6075, https://doi.org/10.1002/smll.201602581.

106. J. Jiu and K. Suganuma, "Metallic Nanowires and Their Application," *IEEE Transactions on Components, Packaging, and Manufacturing Technology* 6, no. 12 (2016): 1733–1751, https://doi.org/10.1109/tcpmt.2016.2581829.

107. W. A. MacDonald, "Latest Advances in Substrates for Flexible Electronics," in *Large Area and Flexible Electronics* (Weinheim: Wiley-VCH Verlag GmbH & Co. KGaA, 2015): 291–314, https://doi.org/10.1002/9783527679973.ch10.

108. V. Zardetto, T. M. Brown, A. Reale, and A. Di Carlo, "Substrates for Flexible Electronics: A Practical Investigation on the Electrical, Film Flexibility, Optical, Temperature, and Solvent Resistance Properties," *Journal of Polymer Science Part B: Polymer Physics* 49, no. 9 (2011): 638–648, https://doi.org/10.1002/polb.22227.

109. M. C. McAlpine, R. S. Friedman, and C. M. Lieber, "High-Performance Nanowire Electronics and Photonics and Nanoscale Patterning on Flexible Plastic Substrates," *Proceedings of the IEEE* 93, no. 7 (2005): 1357–1363, https://doi.org/10.1109/jproc.2005.850308.

110. C. H. Lee, D. R. Kim, and X. Zheng, "Fabricating Nanowire Devices on Diverse Substrates by Simple Transfer-Printing Methods," *Proceedings of the National Academy of Sciences of the United States of America* 107, no. 22 (2010): 9950–9955, https://doi.org/10.1073/pnas.0914031107.

111. E. M. Freer, O. Grachev, X. Duan, S. Martin, and D. P. Stumbo, "High-Yield Self-Limiting Single-Nanowire Assembly With Dielectrophoresis," *Nature Nanotechnology* 5, no. 7 (2010): 525–530, https://doi.org/10.1038/nnano.2010.106.

112. G. Yu, A. Cao, and C. M. Lieber, "Large-Area Blown Bubble Films of Aligned Nanowires and Carbon Nanotubes," *Nature Nanotechnology* 2, no. 6 (2007): 372–377, https://doi.org/10.1038/nnano.2007.150.

113. Y. Huang, X. Duan, Q. Wei, and C. M. Lieber, "Directed Assembly of One-Dimensional Nanostructures Into Functional Networks," *Science* 291, no. 5504 (2001): 630–633, https://doi.org/10.1126/science.291.5504.630.

114. Z. Lou, L. Li, L. Wang, and G. Shen, "Recent Progress of Self-Powered Sensing Systems for Wearable Electronics," *Small* 13, no. 45 (2017): 1701791, https://doi.org/10.1002/smll.201701791.

115. J. Heikenfeld, A. Jajack, J. Rogers, et al., "Wearable Sensors: Modalities, Challenges, and Prospects," *Lab on a Chip* 18, no. 2 (2018): 217–248, https://doi.org/10.1039/c7lc00914c.

116. A. J. Bandodkar, I. Jeerapan, and J. Wang, "Wearable Chemical Sensors: Present Challenges and Future Prospects," *ACS Sensors* 1, no. 5 (2016): 464–482, https://doi.org/10.1021/acssensors.6b00250.

117. Q. Xue, X. Kan, Z. Pan, et al., "An Intelligent Face Mask Integrated With High Density Conductive Nanowire Array for Directly Exhaled Coronavirus Aerosols Screening," *Biosensors and Bioelectronics* 186 (2021): 113286, https://doi.org/10.1016/j.bios.2021.113286.

118. C. G. Nunez, A. Vilouras, W. Taube Navaraj, F. Liu, and R. Dahiya, "ZnO Nanowires-Based Flexible UV Photodetector System for Wearable Dosimetry," *IEEE Sensors Journal* 18, no. 19 (2018): 7881–7888, https://doi.org/10.1109/jsen.2018.2853762.

119. K. Meng, J. Chen, X. Li, et al., "Flexible Weaving Constructed Self-Powered Pressure Sensor Enabling Continuous Diagnosis of Cardiovascular Disease and Measurement of Cuffless Blood Pressure," *Advanced Functional Materials* 29, no. 5 (2018): 1806388, https://doi.org/10.1002/adfm.201806388.

120. K. Huang, J. Liu, S. Lin, et al., "Flexible Silver Nanowire Dry Electrodes for Long-Term Electrocardiographic Monitoring," *Advanced Composites and Hybrid Material* 5, no. 1 (2021): 220–228, https://doi.org/10.1007/s42114-021-00322-0.

121. C. Bell, A. Nammari, P. Uttamchandani, A. Rai, P. Shah, and A. L. Moore, "Flexible Electronics-Compatible Non-Enzymatic Glucose Sensing via Transparent CuO Nanowire Networks on PET Films," *Nanotechnology* 28, no. 24 (2017): 245502, https://doi.org/10.1088/1361-6528/aa7164.

122. L. Shi, J. Feng, Y. Zhu, F. Huang, and K. Aw, "A Review of Flexible Strain Sensors for Walking Gait Monitoring," *Sensors and Actuators A: Physical* 377 (2024): 115730, https://doi.org/10.1016/j.sna.2024.115730.

123. X. Nan, X. Wang, T. Kang, et al., "Review of Flexible Wearable Sensor Devices for Biomedical Application," *Micromachines* 13, no. 9 (2022): 1395, https://doi.org/10.3390/mi13091395.

124. S. Yao, J. Yang, F. R. Poblete, X. Hu, and Y. Zhu, "Multifunctional Electronic Textiles Using Silver Nanowire Composites," *ACS Applied Materials and Interfaces* 11, no. 34 (2019): 31028–31037, https://doi.org/10.1021/acsami.9b07520.

125. S. H. Shin, D. H. Park, J. Y. Jung, M. H. Lee, and J. Nah, "Ferroelectric Zinc Oxide Nanowire Embedded Flexible Sensor for Motion and Temperature Sensing," *ACS Applied Materials and Interfaces* 9, no. 11 (2017): 9233–9238, https://doi.org/10.1021/acsami.7b00380.

126. N. Zhang, Y. Li, S. Xiang, et al., "Imperceptible Sleep Monitoring Bedding for Remote Sleep Healthcare and Early Disease Diagnosis," *Nano Energy* 72 (2020): 104664, https://doi.org/10.1016/j.nanoen.2020.104664.

127. Z. Cui, F. R. Poblete, and Y. Zhu, "Tailoring the Temperature Coefficient of Resistance of Silver Nanowire Nanocomposites and Their Application as Stretchable Temperature Sensors," *ACS Applied Materials and Interfaces* 11, no. 19 (2019): 17836–17842, https://doi.org/10.1021/acsami.9b04045.

128. Z. Yan, S. Zhang, M. Gao, et al., "Ultrasensitive and Wide-Range-Detectable Flexible Breath Sensor Based on Silver Vanadate Nanowires," *ACS Applied Electronic Materials* 5, no. 1 (2023): 520–525, https://doi.org/10.1021/acsaelm.2c01546.

129. M. Zhang, S. Guo, D. Weller, et al., "CdSSe Nanowire-Chip Based Wearable Sweat Sensor," *Journal of Nanobiotechnology* 17, no. 1 (2019): 42, https://doi.org/10.1186/s12951-019-0480-4.

130. S. Zhao, X. Meng, L. Liu, et al., "Polypyrrole-Coated Copper Nanowire-Threaded Silver Nanoflowers for Wearable Strain Sensors With High Sensing Performance," *Chemical Engineering Journal* 417 (2021): 127966, https://doi.org/10.1016/j.cej.2020.127966.

131. Z. Zhao, Q. Li, Y. Dong, J. Gong, and J. Zhang, "Washable Patches With Gold Nanowires/Textiles in Wearable Sensors for Health Monitoring," *ACS Applied Materials and Interfaces* 14, no. 16 (2022): 18884–18900, https://doi.org/10.1021/acsami.2c01729.

132. M. Du, J. Ouyang, and K. Zhang, "Flexible Bi_2Te_3/PEDOT Nanowire Sandwich-Like Films Towards High-Performance Wearable Cross-Plane Thermoelectric Generator and Temperature Sensor Array," *Journal of Materials Chemistry A* 11, no. 30 (2023): 16039–16048, https://doi.org/10.1039/d3ta02876c.

133. S. Huang, B. Zhang, Z. Shao, et al., "Ultraminiaturized Stretchable Strain Sensors Based on Single Silicon Nanowires for Imperceptible Electronic Skins," *Nano Letters* 20, no. 4 (2020): 2478–2485, https://doi.org/10.1021/acs.nanolett.9b05217.

134. H. Cui, S. Li, S. Deng, H. Chen, and C. Wang, "Flexible, Transparent, and Free-Standing Silicon Nanowire SERS Platform for In Situ Food Inspection," *ACS Sensors* 2, no. 3 (2017): 386–393, https://doi.org/10.1021/acssensors.6b00712.

135. S. Huang, B. Zhang, Y. Lin, C. S. Lee, and X. Zhang, "Compact Biomimetic Hair Sensors Based on Single Silicon Nanowires for Ultrafast and Highly-Sensitive Airflow Detection," *Nano Letters* 21, no. 11 (2021): 4684–4691, https://doi.org/10.1021/acs.nanolett.1c00852.

136. J. L. Mead, S. Wang, S. Zimmermann, S. Fatikow, and H. Huang, "Resolving the Adhesive Behavior of 1D Materials: A Review of Experimental Approaches," *Engineering* 24 (2023): 39–72, https://doi.org/10.1016/j.eng.2023.02.012.

137. F. R. Poblete, Z. Cui, Y. Liu, and Y. Zhu, "Stretching Nanowires on a Stretchable Substrate: A Method Towards Facile Fracture Testing and Elastic Strain Engineering," *Extreme Mechanics Letters* 41 (2020): 101035, https://doi.org/10.1016/j.eml.2020.101035.

138. R. Yuan, W. Qian, Y. Zhang, et al., "Orthogonal-Stacking Integration of Highly Conductive Silicide Nanowire Network as Flexible and Transparent Thin Films," *Advanced Electronic Materials* 9, no. 7 (2023): 2201185, https://doi.org/10.1002/aelm.202201185.

139. R. Yuan, W. Qian, Z. Liu, et al., "Designable Integration of Silicide Nanowire Springs as Ultra-Compact and Stretchable Electronic Interconnections," *Small* 18, no. 6 (2022): e2104690, https://doi.org/10.1002/smll.202104690.

140. K. Värbu, N. Muhammad, and Y. Muhammad, "Past, Present, and Future of EEG-Based BCI Applications," *Sensors* 22, no. 9 (2022): 3331, https://doi.org/10.3390/s22093331.

141. S. Steinert, C. Bublitz, R. Jox, and O. Friedrich, "Doing Things With Thoughts: Brain-Computer Interfaces and Disembodied Agency," *Philosophy & Technology* 32, no. 3 (2018): 457–482, https://doi.org/10.1007/s13347-018-0308-4.

142. U. Chaudhary, N. Birbaumer, and A. Ramos-Murguialday, "Brain-Computer Interfaces in the Completely Locked-In State and Chronic Stroke," *Progress in Brain Research* 228 (2016): 131–161, https://doi.org/10.1016/bs.pbr.2016.04.019.

143. D. J. McFarland, J. Daly, C. Boulay, and M. A. Parvaz, "Therapeutic Applications of BCI Technologies," *Brain Computer Interfaces (Abingdon, England)* 47, no. 1–2 (2017): 37–52, https://doi.org/10.1080/2326263X.2017.1307625.

144. C. Marquez-Chin, A. Marquis, and M. R. Popovic, "BCI-Triggered Functional Electrical Stimulation Therapy for Upper Limb," *European Journal of Translational Myology* 26, no. 3 (2016): 6222, https://doi.org/10.4081/ejtm.2016.6222.

145. M. Kang, S. Jung, H. Zhang, et al., "Subcellular Neural Probes From Single-Crystal Gold Nanowires," *ACS Nano* 8, no. 8 (2014): 8182–8189, https://doi.org/10.1021/nn5024522.

146. C. Lu, S. Park, T. J. Richner, et al., "Flexible and Stretchable Nanowire-Coated Fibers for Optoelectronic Probing of Spinal Cord Circuits," *Science Advances* 3, no. 3 (2017): e1600955, https://doi.org/10.1126/sciadv.1600955.

147. M. Ryu, J. H. Yang, Y. Ahn, et al., "Enhancement of Interface Characteristics of Neural Probe Based on Graphene, ZnO Nanowires, and Conducting Polymer PEDOT," *ACS Applied Materials and Interfaces* 9, no. 12 (2017): 10577–10586, https://doi.org/10.1021/acsami.7b02975.

148. S. Lin, J. Liu, W. Li, et al., "A Flexible, Robust, and Gel-Free Electroencephalogram Electrode for Noninvasive Brain-Computer Interfaces," *Nano Letters* 19, no. 10 (2019): 6853–6861, https://doi.org/10.1021/acs.nanolett.9b02019.

149. S. Oh, P. S. Kumar, H. Kwon, and V. K. Varadan, "Wireless Brain-Machine Interface Using EEG and EOG: Brain Wave Classification and Robot Control," *Nanosensors, Biosensors, and Info-Tech Sensors and Systems 2012* 8344 (2012): 160–167, https://doi.org/10.1117/12.918159.

150. A. Zhang, Y. Zhao, S. S. You, and C. M. Lieber, "Nanowire Probes Could Drive High-Resolution Brain-Machine Interfaces," *Nano Today* 31 (2020): 100821, https://doi.org/10.1016/j.nantod.2019.100821.

151. J. P. Neto, A. Costa, J. Vaz Pinto, et al., "Transparent and Flexible Electrocorticography Electrode Arrays Based on Silver Nanowire Networks for Neural Recordings," *ACS Applied Nano Materials* 4, no. 6 (2021): 5737–5747, https://doi.org/10.1021/acsanm.1c00533.

152. X. Yang, T. Zhou, T. J. Zwang, et al., "Bioinspired Neuron-Like Electronics," *Nature Materials* 18, no. 5 (2019): 510–517, https://doi.org/10.1038/s41563-019-0292-9.

153. M. T. Almansoori, X. Li, and L. Zheng, "A Brief Review on E-Skin and Its Multifunctional Sensing Applications," *Current Smart Materials.* 4, no. 1 (2019): 3–14, https://doi.org/10.2174/2405465804666190313154903.

154. A. S. Dolbashid, M. S. Mokhtar, F. Muhamad, and F. Ibrahim, "Potential Applications of Human Artificial Skin and Electronic Skin (E-Skin): A Review," *Bioinspired, Biomimetic and Nanobiomaterials* 7, no. 1 (2018): 53–64, https://doi.org/10.1680/jbibn.17.00002.

155. Q. J. Sun, Q. T. Lai, Z. Tang, X. Tang, X. Zhao, and V. A. L. Roy, "Advanced Functional Composite Materials toward E-Skin for Health Monitoring and Artificial Intelligence," *Advanced Materials Technologies* 8, no. 5 (2022): 2201088, https://doi.org/10.1002/admt.202201088.

156. B. Nie, S. Liu, Q. Qu, Y. Zhang, M. Zhao, and J. Liu, "Bio-Inspired Flexible Electronics for Smart E-Skin," *Acta Biomaterialia* 139 (2022): 280–295, https://doi.org/10.1016/j.actbio.2021.06.018.

157. M. S. Suen, Y. C. Lin, and R. Chen, "A Flexible Multifunctional Tactile Sensor Using Interlocked Zinc Oxide Nanorod Arrays for Artificial Electronic Skin," *Sensors and Actuators A: Physical* 269 (2018): 574–584, https://doi.org/10.1016/j.sna.2017.11.053.

158. Y. Li, D. Han, C. Jiang, E. Xie, and W. Han, "A Facile Realization Scheme for Tactile Sensing With a Structured Silver Nanowire-PDMS Composite," *Advanced Materials Technologies* 4, no. 3 (2018): 1800504, https://doi.org/10.1002/admt.201800504.

159. Y. Zhang, Y. Fang, J. Li, et al., "Dual-Mode Electronic Skin With Integrated Tactile Sensing and Visualized Injury Warning," *ACS Applied Materials and Interfaces* 9, no. 42 (2017): 37493–37500, https://doi.org/10.1021/acsami.7b13016.

160. J. Ge, L. Sun, F. R. Zhang, et al., "A Stretchable Electronic Fabric Artificial Skin With Pressure-Lateral Strain- and Flexion-Sensitive Properties," *Advances in Materials* 28, no. 4 (2016): 722–728, https://doi.org/10.1002/adma.201504239.

161. S. Gong, Y. Wang, L. W. Yap, et al., "A Location- and Sharpness-Specific Tactile Electronic Skin Based on Staircase-Like Nanowire Patches," *Nanoscale Horizons* 3, no. 6 (2018): 640–647, https://doi.org/10.1039/c8nh00125a.

162. K. Takei, T. Takahashi, J. C. Ho, et al., "Nanowire Active-Matrix Circuitry for Low-Voltage Macroscale Artificial Skin," *Nature Materials* 9, no. 10 (2010): 821–826, https://doi.org/10.1038/nmat2835.

163. Y. Du, P. Shen, H. Liu, et al., "Multi-Receptor Skin With Highly Sensitive Tele-Perception Somatosensory," *Science Advances* 10, no. 37 (2024): eadp8681, https://doi.org/10.1126/sciadv.adp8681.

164. S. Gong, L. W. Yap, B. Zhu, et al., "Local Crack-Programmed Gold Nanowire Electronic Skin Tattoos for In-Plane Multisensor Integration," *Advances in Materials* 31, no. 41 (2019): e1903789, https://doi.org/10.1002/adma.201903789.

165. C. Zhao, Y. Fang, H. Chen, et al., "Ultrathin Mo_2S_3 Nanowire Network for High-Sensitivity Breathable Piezoresistive Electronic Skins," *ACS Nano* 17, no. 5 (2023): 4862–4870, https://doi.org/10.1021/acsnano.2c11564.

166. Y. Wang, S. Lee, T. Yokota, et al., "A Durable Nanomesh On-Skin Strain Gauge for Natural Skin Motion Monitoring With Minimum Mechanical Constraints," *Science Advances* 6, no. 33 (2020): eabb7043, https://doi.org/10.1126/sciadv.abb7043.

167. Q. Liu, Z. Liu, C. Li, et al., "Highly Transparent and Flexible Iontronic Pressure Sensors Based on an Opaque to Transparent Transition," *Advanced Science* 7, no. 10 (2020): 2000348, https://doi.org/10.1002/advs.202000348.

168. P. K. Nayak, L. Yang, W. Brehm, and P. Adelhelm, "From Lithium-Ion to Sodium-Ion Batteries: Advantages, Challenges, and Surprises," *Angewandte Chemie International Edition* 57, no. 1 (2018): 102–120, https://doi.org/10.1002/anie.201703772.

169. B. Diouf and R. Pode, "Potential of Lithium-Ion Batteries in Renewable Energy," *Renewable Energy* 76 (2015): 375–380, https://doi.org/10.1016/j.renene.2014.11.058.

170. M. Walter, M. V. Kovalenko, and K. V. Kravchyk, "Challenges and Benefits of Post-Lithium-Ion Batteries," *New Journal of Chemistry* 44, no. 5 (2020): 1677–1683, https://doi.org/10.1039/C9NJ05682C.

171. N. Yabuuchi, K. Kubota, M. Dahbi, and S. Komaba, "Research Development on Sodium-Ion Batteries," *Chemistry Review* 114, no. 23 (2014): 11636–11682, https://doi.org/10.1021/cr500192f.

172. M. Al-Amin, S. Islam, S. U. A. Shibly, and S. Iffat, "Comparative Review on the Aqueous Zinc-Ion Batteries (AZIBs) and Flexible Zinc-Ion Batteries (FZIBs)," *Nanomaterials* 12, no. 22 (2022): 3997, https://doi.org/10.3390/nano12223997.

173. P. Yu, Y. Zeng, H. Zhang, M. Yu, Y. Tong, and X. Lu, "Flexible Zn-Ion Batteries: Recent Progresses and Challenges," *Small* 15, no. 7 (2019): e1804760, https://doi.org/10.1002/smll.201804760.

174. X. Zhu, H. Zhang, Y. Huang, et al., "Recent Progress of Flexible Rechargeable Batteries," *Science Bulletin* 69, no. 23 (2024): 3730–3755, https://doi.org/10.1016/j.scib.2024.09.032.

175. Q. Liu, Z. Chang, Z. Li, and X. Zhang, "Flexible Metal–Air Batteries: Progress, Challenges, and Perspectives," *Small Methods* 2, no. 2 (2017): 1700231, https://doi.org/10.1002/smtd.201700231.

176. Y. Wang, Y. Sun, W. Ren, et al., "Challenges and Prospects of Mg-Air Batteries: A Review," *Energy Materials* 2, no. 4 (2022): 200024, https://doi.org/10.20517/energymater.2022.20.

177. W. Fu, K. Turcheniuk, O. Naumov, et al., "Materials and Technologies for Multifunctional, Flexible or Integrated Supercapacitors and Batteries," *Materials Today* 48 (2021): 176–197, https://doi.org/10.1016/j.mattod.2021.01.026.

178. M. R. Benzigar, V. D. B. C. Dasireddy, X. Guan, T. Wu, and G. Liu, "Advances on Emerging Materials for Flexible Supercapacitors: Current Trends and Beyond," *Advanced Functional Materials* 30, no. 40 (2020): 2002993, https://doi.org/10.1002/adfm.202002993.